



Seismic stratigraphy along the Amundsen Sea to Ross Sea continental rise: A cross-regional record of pre-glacial to glacial processes of the West Antarctic margin



Ansa Lindeque^{a,*}, Karsten Gohl^a, Stuart Henrys^b, Florian Wobbe^a, Bryan Davy^b

^a Alfred-Wegener-Institut Helmholtz-Zentrum für Polar- und Meeresforschung, Am Alten Hafen 26, 27568 Bremerhaven, Germany

^b GNS Science, 1 Fairway Drive, Avalon, Lower Hut 5010, New Zealand

ARTICLE INFO

Article history:

Received 8 June 2015

Received in revised form 10 November 2015

Accepted 17 November 2015

Available online 26 November 2015

Keywords:

West Antarctica

Seismic stratigraphy

Glacial development

Bottom-currents

Sediment thickness

ABSTRACT

The seismic sediment record of the Amundsen Sea continental rise provides insight into the sedimentation processes from pre-glacial to glacial times, variations in ocean-bottom circulation, early ice sheet growth, and intensification towards the present icehouse regime. Seismic reflection data acquired during the 2010 RV *Polarstern* and the 2006 RV *Tangaroa* expeditions, created a >2000 km long continuous Amundsen Sea to Ross Sea seismic transect. Pre-existing lines linked to this transect, connect key seismic stratigraphy horizons from the Ross Sea shelf to the rise and farther along the West Antarctic margin, up to the Amundsen Sea Embayment. Seismic units AS-1 to AS-3 constitute the Cretaceous to Eocene pre-glacial (PG) sequence (79–34 Ma), units AS-4 to AS-6 the Eocene to mid-Miocene transitional (T) sequence (34–15.5 Ma), and units AS-7 to AS-11 the mid-Miocene to Quaternary full glacial (FG) climate sequence (15.5–0 Ma). The top PG sequence boundary horizon AS-u3/uPG-T, links to unconformity RSU6 of the Ross Sea shelf and to the base of Unit II of the eastern Amundsen Sea, and is interpreted as the first arrival of grounded ice on the shelf. The top T sequence boundary AS-u6/uT-FG, links to RSU4 and the base of Unit III, and is interpreted as the onset of the FG regime with intensified ice sheet advances onto the outer shelves. The Amundsen Sea basin accumulated up to 3.9 km thick sediments in its centre. Seismic facies geometry analysis suggests Paleocene–Eocene bottom-current activity, late Eocene shelf grounding of the West Antarctic Ice Sheet, and no apparent difference in the deep-sea sediment transport processes or temporal shift in deposition between the Amundsen Sea and Ross Sea. Implications for a Marie Byrd Land uplift starting at ~30 Ma are observed by a progressive change in horizon dip in the central Amundsen Sea seismic sequences.

© 2015 The Authors. Published by Elsevier B.V. This is an open access article under the CC BY license (<http://creativecommons.org/licenses/by/4.0/>).

1. Introduction

West Antarctica has played a vital role in palaeoenvironmental and palaeoclimate processes due to its low-lying topography sculpted by West Antarctic Rift System Cenozoic tectonics and crustal thinning. It hosts an ice sheet of 3–5 m sea-level equivalent (Bamber et al., 2009; Fretwell et al., 2013) that is potentially vulnerable to global warming and likely to be affected by changes in global ocean circulation (e.g. Pritchard et al., 2012). The answers to an improved understanding of West Antarctica's palaeoenvironmental and glacial history from the Greenhouse world to the Neogene and Quaternary glacial periods lie largely in the offshore sedimentary records.

The sedimentary record off the Pacific margin of West Antarctica captured the last 90 million years of syn- to post-breakup pre-glacial evolution, the earliest Antarctic glaciation, ice sheet development and ocean circulation history. At the stages where continental-scale ice sheets began to expand and grounded on the continental shelf, erosion and rapid transport moved large amounts of sediments from inland to the coast, shelf, slope, and deep-sea. Such increased sediment supply and changes in transport/depositional processes combine to form sedimentary features that can be identified in seismic reflection images. The characteristics of these features, such as the geometry and reflectivity, can be related back to a general depositional environment or process (e.g. Shanmugam, 2006).

Whilst records for Antarctic sediment supply and deposition processes have been studied via marine seismic reflection images around Antarctic continental rises (e.g. Nitsche et al., 1997, 2000; De Santis et al., 2003; Rogenhagen et al., 2004; Escutia et al., 2005, 2011; Maldonado et al., 2006; Scheuer et al., 2006; Leitchenkov et al., 2007a, b; Uenzelmann-Neben and Gohl, 2012, 2014; Lindeque et al., 2013), the Marie Byrd Land sector of the southern Pacific between the Ross

* Corresponding author at: TGS Geophysical Company (UK) Limited, 1 The Crescent, Surbiton, Surrey KT6 4BN, United Kingdom. Tel.: +44 744 3833836.

E-mail addresses: ansa.lindeque@icloud.com (A. Lindeque), karsten.gohl@awi.de (K. Gohl), s.henrys@gns.cri.nz (S. Henrys), florian.wobbe@awi.de (F. Wobbe), B.Davy@gns.cri.nz (B. Davy).

Sea and the eastern Amundsen Sea basin remains largely unexplored. Thus its contribution to the West Antarctic sediment budget from pre-glacial to glacial times is unknown. Knowledge of such sediment budgets are important, for instance, to improve reconstructions of Antarctic palaeo-topographies at times of climatic relevance (Wilson et al., 2012) and to constrain boundary conditions for palaeo-ice sheet models (Wilson et al., 2013). Other important questions addressed by studying the sedimentary record of the Amundsen Sea and eastern Ross Sea continental rises include:

- Which part of the sediment record indicates the location and time of the onset of the glacially dominated environment of West Antarctica?
- Where are the major deposition centres for the pre-glacial to glacial periods, and what processes may have caused their formation?
- Is there a difference in the deep-sea sediment transport processes or a shift in deposition between the Amundsen Sea and Ross Sea, and if so why?
- What evidence is there to reveal the development of past bottom current formation?
- Is there regional variation in the acoustic basement topography and if so, what can it reveal about the tectonic history of the Amundsen Sea basin development?

Acquisition of seismic reflection data on the Ross Sea continental rise in 2006 (RV *Tangaroa* survey TAN-2006; Fig. 1) and along a ~2000 km transect from the eastern Ross Sea to the eastern Amundsen Sea

continental rise in 2010 (RV *Polarstern* expedition ANT-XXVI/3, the AWI-2010 survey in Fig. 1; Gohl, 2010) provide the first seismic link across the previously unsurveyed central and western Amundsen Sea sector (115°W to 170°W; Fig. 1). This dataset now presents an opportunity to establish a direct seismic horizon stratigraphic correlation between the two major West Antarctic Ice Sheet (WAIS) drainage outlet basins – the Ross Sea and Amundsen Sea embayments – to address these open questions.

In this work, we use the generally accepted partition of three major Antarctic climate regimes in the Cenozoic (e.g. Lindeque et al., 2013): The pre-glacial climate regime is defined as being relatively warm and predominantly ice sheet free, except for smaller glaciers in high altitudes, and open-ocean conditions without major sea-ice cover. The transitional regime refers to a colder climate, analogous to the present day Alpine climates with regional scale ice sheets undergoing multiple advance/retreat cycles to and from coastal areas and inner shelves, and only perennial regional sea-ice cover. The full glacial climate regime describes a climate similar to present day West Antarctica, in which continental scale ice sheets expanded to the coastal regions and grounded on the middle to outer shelf during glacial maxima.

2. Tectonic and palaeoenvironmental setting

2.1. Rifting and basin development

The Amundsen Sea basin formation started in the late Cretaceous during continental rifting, before initial oceanic crust formed, when

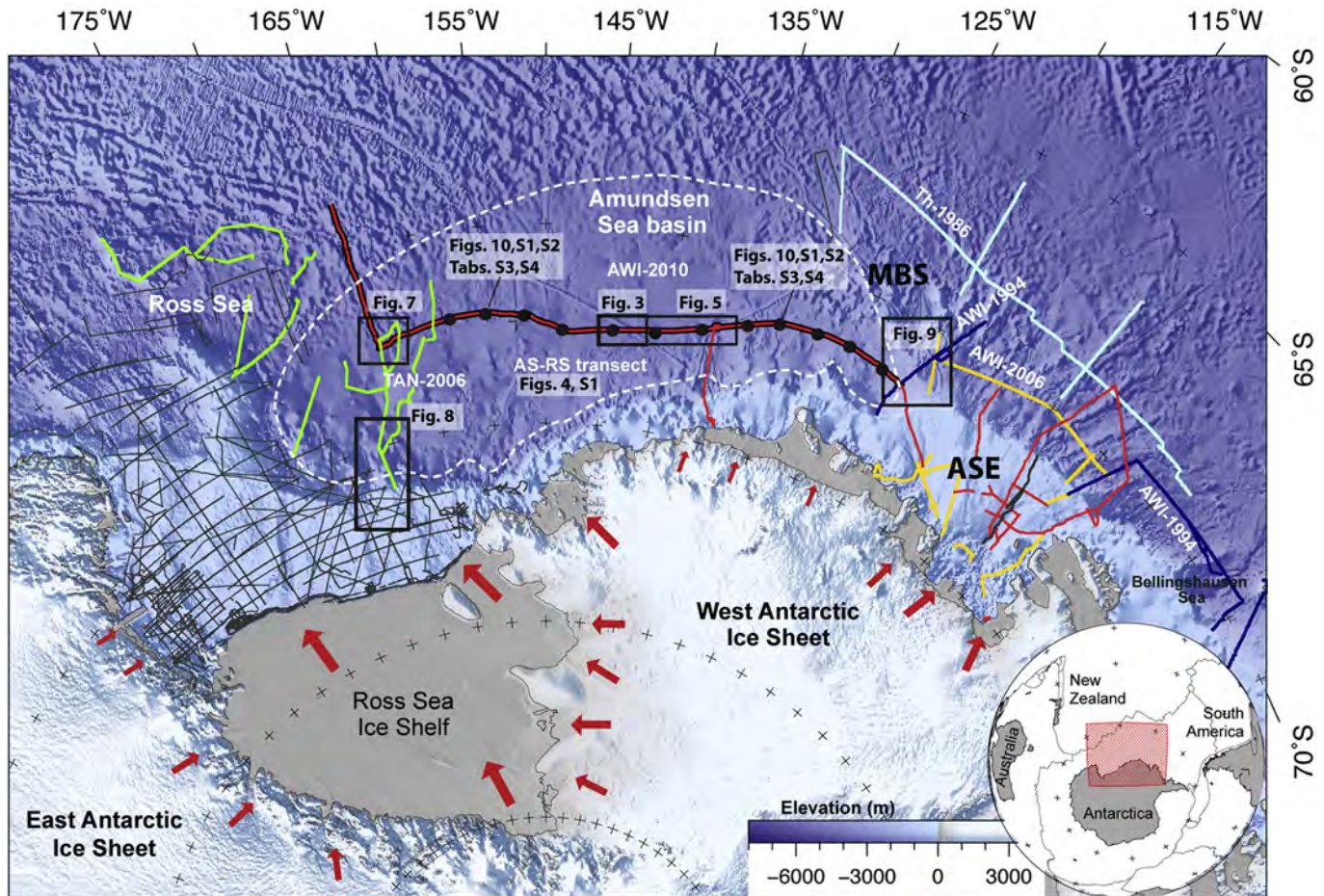


Fig. 1. Overview map of the Amundsen Sea to Ross Sea study area with seismic surveys referred to in this paper demarcated as: AWI-2010—red; TAN-2006—green; AWI-2006—yellow; AWI-1994—navy; other lines are TH86—light blue, and on the Ross Sea shelf—grey. The AS-RS transect is shown in the thick black/red line (Fig. 4; Fig. S1). The black dots represent the 12 points used for the sediment thickness estimates (Figs. 4, 10; Fig. S2; Tables S3, S4). The background image is the International Bathymetric Chart of the Southern Ocean (Arndt et al., 2013). Red arrows indicate the general ice flow drainage directions of the West Antarctic Ice Sheet (WAIS) and East Antarctic Ice Sheet (EAIS) after Bamber et al. (2009). MBS—Marie Byrd Seamounts; ASE—Amundsen Sea Embayment. (For interpretation of the references to colour in this figure legend, the reader is referred to the web version of this article.)

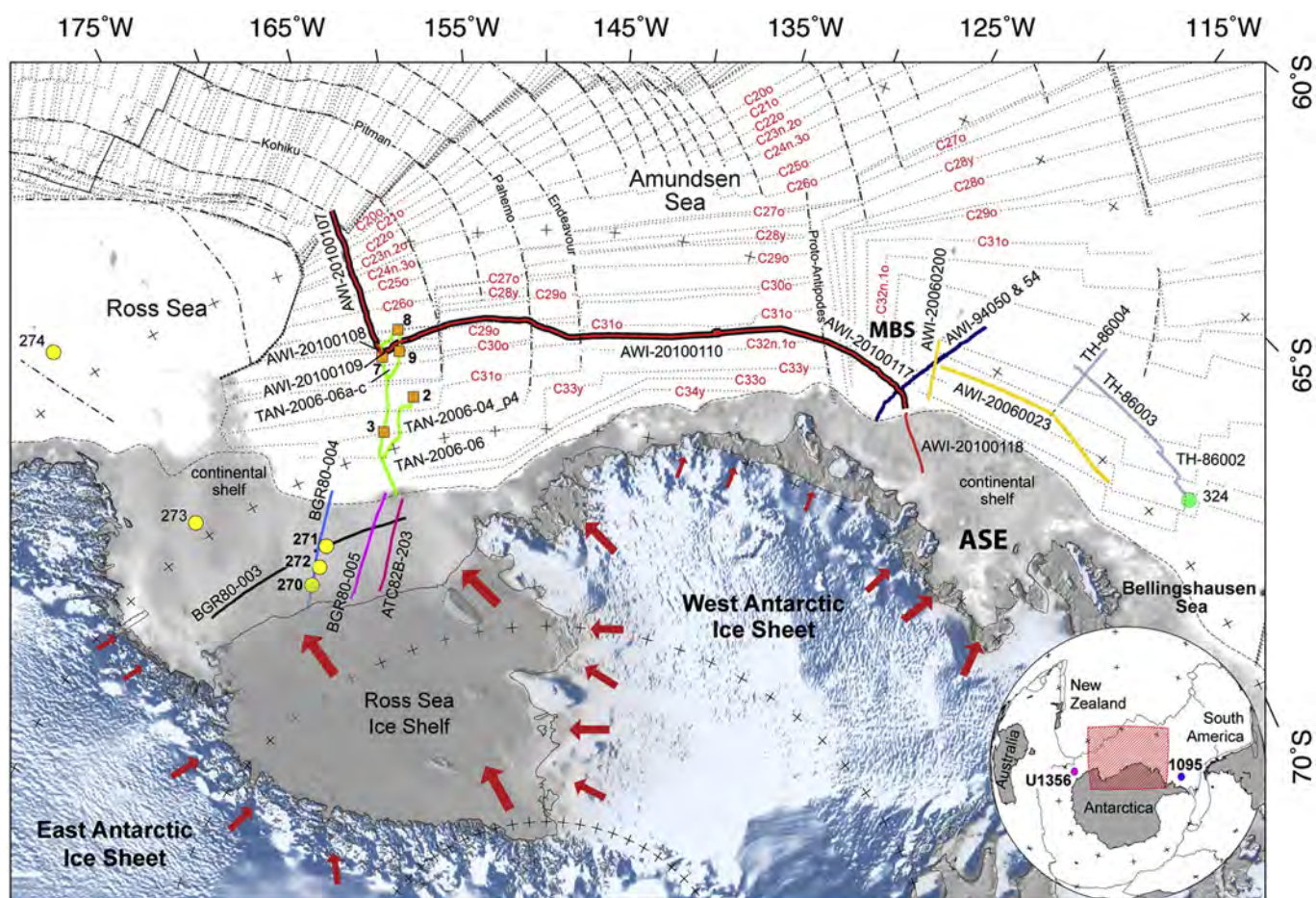


Fig. 2. Isochron compilation map for the Amundsen Sea and Ross Sea region modified after Wobbe et al. (2012). Isochrons are labelled in red and appended with o—old or y—young. Dashed lines are fracture zones (FZ) that cross the AS–RS transect (thick red/black line). Selected tie lines used in this work are annotated and summarised in Table S2. Main seismic surveys are AWI-2010—red; TAN-2006—green; AWI-2006—yellow; AWI-1994—navy; selected lines from BGR80—labelled. Supporting age information was drawn from boreholes: yellow circles—DSDP Leg 28 Sites 270 to 274; green circle—DSDP Leg 35 Site 324; and shown on the inset: blue circle—ODP Leg 178 Site 1095; purple circle—IODP Leg 318 Sites U1356 and U1359. Velocity data for sediment thickness estimates were taken from: selected TAN-2006 sonobuoys—orange squares (supp. Fig. S2); interval velocities from the AS–RS transect seismic data (Tables S3, S4; Fig. S2); and ocean-bottom seismograph (OBS) measurements on line AWI-20060200 (Kalberg and Gohl, 2014). MBS—Marie Byrd Seamounts; ASE—Amundsen Sea Embayment. Red arrows—as in Fig. 1. (For interpretation of the references to colour in this figure legend, the reader is referred to the web version of this article.)

the Campbell Plateau and Chatham Rise of New Zealand separated from the Pacific margin of West Antarctica at western Thurston Island and Marie Byrd Land, between 90 and 83 Ma (Fig. 2; Table S1; e.g. Eagles et al., 2004a; Wobbe et al., 2012). The basin opening propagated from east to west. In the east, multi-stage wide-mode rifting dominated in the Amundsen Sea Embayment (Wobbe et al., 2012; Kalberg and Gohl, 2014), whilst narrow-mode extension took place in the eastern Ross Sea and off western Marie Byrd Land (Luyendyk et al., 2003; Davey and De Santis, 2006; Jordan et al., 2010).

Between about 80 and 62 Ma (C34y and c27o in Fig. 2), the Bellingshausen Plate moved independently from the Antarctic Plate east of the Proto-Antipodes Fracture Zone (FZ) (Fig. 2; Table S1; Larter et al., 2002; Eagles et al., 2004a,b; Wobbe et al., 2012). The southern margin of the Bellingshausen Plate formed a diffuse, possibly distributed plate boundary zone crossing the Amundsen Sea Embayment (Fig. 2; Wobbe et al., 2012). By 61 Ma, the Bellingshausen Plate was incorporated into the Antarctic Plate (Table S1; Cande et al., 2000; Eagles et al., 2004a,b; Wobbe et al., 2012).

Shortly after, or concurrent with the Bellingshausen Plate demise, the Marie Byrd Seamounts (Figs. 1, 2) were emplaced at about 65–56 Ma. (Kipf et al., 2014; Table S1). Recent gravity and seismic refraction data modelling of the Amundsen Sea Embayment and eastern Amundsen Sea continental rise (line AWI-20060200, Fig. 2) suggest that the Marie Byrd Seamount emplacement was accompanied by magmatic underplating due to partial melting (Kalberg and Gohl, 2014). The

remaining Oligocene, Eocene and Miocene stages of the basin development comprised on-going passive margin rifting.

2.2. Palaeoenvironmental development

A comprehensive chronology of palaeoclimatic events is compiled in Table S1. The following events are most relevant and intertwined with sedimentation processes along the Pacific margin of West Antarctica:

The Cretaceous–Palaeocene climate is thought to have been warm and relatively ice-free. Most of West Antarctica was elevated above sea level (Wilson et al., 2012) and the ocean gateways between East Antarctica and Australia (Tasmanian gateway), and between South America and the Antarctic Peninsula (Drake Passage/Scotia Sea gateway) were still closed (e.g. Bijl et al., 2013; Eagles and Jokat, 2014). A proto Amundsen Sea–Ross Sea gyre may have developed towards the late Palaeocene (Huber et al., 2004) when surface waters cooled sufficiently to initiate bottom water circulation (Uenzelmann-Neben and Gohl, 2012).

In the Late Eocene, shallow to deep water passages developed in the Tasmanian and Drake Passage/Scotia Sea gateways, and Antarctica's climate became increasingly cooler. By the Eocene–Oligocene transition, the first continent-wide West Antarctic Ice Sheet (WAIS) is likely to have formed (Wilson et al., 2013; Olivetti et al., 2015). It also has been hypothesised that bottom currents in the Amundsen Sea intensified

during this time, favouring the formation of elongate sediment drifts in the eastern sector (Uenzelmann-Neben and Gohl, 2012).

U–Pb geochronology on detrital apatite grains in the Cape Roberts Projects (CRP) drill cores of the western Ross Sea provides indications for an Oligocene ice sheet with occasional grounding and expansion onto the Ross Sea shelf (Olivetti et al., 2015). They argue that it is a record from the WAIS, although we think it is a combined record from both the EAIS and the WAIS. Compared to 70 Ma, the 34 Ma Oligocene West Antarctica topography has been significantly eroded and a great fraction of the present-day Ross Sea shelf submerged (Wilson et al., 2012, 2013). The Eocene–Oligocene transition is marked by high amplitude regional unconformities, visible in the Ross Sea and Wilkes Land margin seismic images (De Santis et al., 1999; Escutia et al., 2005). However, the extent of the Eocene–Oligocene transition is not well constrained on the Antarctic continental margin due to the paucity of drill samples. In Wilson et al. (2012), for example, a large range of WAIS extension at the Eocene–Oligocene boundary is given.

In the Oligocene, the Southern Ocean gateways opened deep-water passages and the Antarctic Circumpolar Current (ACC) developed. This period is marked by an increased amount of sediment deposition, e.g. seismic units RSS-3 and RSS-4 in the Ross Sea (Brancolini et al., 1995; De Santis et al., 1999; Brancolini and Leitchenkov, 2010), WL-S5 and WL-S4 off Wilkes Land margin (De Santis et al., 2003; Escutia et al., 2005, 2011) and Unit II in the eastern Amundsen Sea (Uenzelmann-Neben and Gohl, 2012; Table S1). Elongate drifts and channel–levee drift deposits in the eastern Amundsen Sea increased in response to intensified bottom water circulation (Uenzelmann-Neben and Gohl, 2012). In addition, sediment transport across the shelf and slope increased due to the numerous advance cycles of the continental-scale ice sheets expanding towards the coast, and partially onto the inner shelves (Brancolini et al., 1995; De Santis et al., 1999; Haywood et al., 2009; Brancolini and Leitchenkov, 2010; Uenzelmann-Neben and Gohl, 2012; Gohl et al., 2013).

The mid-Miocene to Quaternary period is dominated by the intensified and more frequent advance and retreat cycles of the Antarctic ice sheets onto the middle and outer shelves (e.g. Miller et al., 2008), and the building of progradational shelf sequences (De Santis et al., 1999; Brancolini and Leitchenkov, 2010; Gohl et al., 2013). During this period, the ACC and Antarctic Bottom Water (AABW) circulation developed fully (Uenzelmann-Neben and Gohl, 2012; Table S1). The Antarctic topography gradually changed, especially in the West Antarctic and in the Ross Sea, where much of the region became submerged (Wilson et al., 2012, 2013) to approach the present day topography (Fretwell et al., 2013). Signatures of these changes on the continental rise of West Antarctica, are recorded in seismic units RSS-5 to RSS-8 of the eastern Ross Sea (Brancolini et al., 1995; De Santis et al., 1999; Brancolini and Leitchenkov, 2010), WL-S9 off Wilkes Land (De Santis et al., 2003; Escutia et al., 2005, 2011), and Units III and IV in the eastern Amundsen Sea (Uenzelmann-Neben and Gohl, 2012).

3. Database and methods

3.1. Seismic reflection data

The multichannel seismic profiles AWI-2010xxxx used to construct the Amundsen Sea to Ross Sea (AS–RS) transect were acquired during the RV *Polarstern* expedition ANT-XXVI/3 in 2010 (Figs. 1, 2; Table S2; Gohl, 2010). Exceptionally favourable sea-ice conditions allowed the acquisition of a continuous ~2000 km long profile along the 72°S latitude. The TAN-2006-xx lines (Figs. 1, 2; Table S2) were acquired during the RV *Tangaroa* expedition in 2006 (hereafter referred to as the TAN-2006 survey) and complement the AWI lines (hereafter referred to as the AWI-2010 survey). This combined dataset links pre-existing seismic data of the continental rise and shelf of the eastern Amundsen Sea (e.g. Nitsche et al., 1997, 2000; Scheuer et al., 2006; Uenzelmann-Neben and Gohl, 2012, 2014; Gohl et al., 2013) with data

from the Ross Sea rise and shelf (e.g. Anderson and Bartek, 1992; ANTOSTRAT, 1995; Brancolini et al., 1995; De Santis et al., 1995, 1999; Brancolini and Leitchenkov, 2010). The acquisition and processing parameters of the AWI-2010 and the TAN-2006 survey data are described below and listed in Table S2 for lines used in this work.

3.1.1. The AWI-2010 survey of RV *Polarstern*

Most of the AWI-2010 profiles (Figs. 1, 2; Table S2) were acquired using a 3000 m long SERCEL Sentinel solid streamer with 240 active channels, towed at a nominal water-depth of 10 m. Profiles AWI-20100108 and AWI-20100109 are the exceptions, where the long streamer was replaced with an older, analogue 600 m long Prakla streamer with 96 channels due to adverse sea-ice conditions. These two profiles are shorter (34 km and 54 km respectively, Table S2) and have a minimal impact on the overall transect data quality or continuity. In all cases, the seismic source consisted of two or three GI-Guns of 4.8–7.2 L (300–450 in³) total volume, fixed to a steel frame and towed in about 3 m water-depth (Table S2). Shots were fired at a 12 s interval in true GI-mode and with 19.5 MPa nominal operational pressure. Data were sampled at a 1 ms interval and recorded for 10 s. Restrictions by the German Federal Environmental Agency prevented the use of a larger airgun source needed to image the basement beneath very thick sedimentary layers. Consequently, basement was poorly imaged in some cases, especially in the easternmost part of profile AWI-20100117.

Seismic processing followed a standard approach using the processing software FOCUS/ECHOS (by Paradigm). After trace editing, a high-pass filter tapered at 5–10 Hz was applied to allow higher frequencies and maximum resolution of the data. Predictive and spiking deconvolution were tested to remove the ghost and internal multiples prior to velocity analyses. Spiking deconvolution effectively removed the ghost when using a 30 ms window, 100 ms operator length and 0.1% white noise, but introduced ringing artefacts in key parts of the deeper sequences and across major sequence boundaries after stacking. It was therefore only applied during velocity analyses and in selected cases, to more clearly image unconformities, drifts feature geometry or the seismic unit boundaries. Static corrections of up to 2 ms were applied to profiles AWI-20100108 and -109, because the 600 m streamer was not equipped with depth-control devices due to sea-ice. The ghost on these two profiles was effectively removed with the application of an F-K filter.

Velocity analysis was applied at every 50th CDP and intervals were picked to match sequence boundary horizons closely. After normal-move-out (NMO) correction and spherical divergence adjustment, a Kirchhoff time-migration was applied to the stacked section. A maximum migration angle of 65° and 90% of the NMO velocities were used.

The interpretation of the seismic images is based on the change in seismic characteristics such as reflectivity and variation of internal reflection geometries. No additional filters or amplitude scaling were applied to most sections, so that true amplitudes were largely preserved. In one case, Automatic Gain Control (AGC) was partially applied on line AWI-20100117 between CDPs 15000 and 22988 to image the basement more clearly.

3.1.2. The TAN-2006 survey of RV *Tangaroa*

The RV *Tangaroa* acquired 3409 km of multichannel seismic data and velocity data from 16 sonobuoys during the TAN-2006 marine geophysical survey in the Ross Sea, conducted by NIWA and GNS Science of New Zealand (Fig. 1; Table S2). Eleven seismic lines were acquired with a 300 m streamer with 48 channels (near offset ~129 m and far-offset ~422 m) towed at a nominal depth of 10 m. The source consisted of 4 GI-Guns (9.8 L) towed at 5 m depth and fired in true GI-mode, resulting in a shot spacing of 50 m. Recording was done for 12 s at a sample interval of 1 ms and a 10 Hz low-cut filter applied during acquisition.

The lines vary in geometry and acquisition parameters due to sea-ice conditions, which introduced additional noise and necessitated processing in parts. This particularly affected line TAN-2006-04, where noise

from sea-ice conditions and damage caused by the snagging and parting of the streamer by an iceberg, reduced sections of the 48 channel streamer to 16 channels on the whole array (Table S2).

Preliminary seismic data processing to final migrated stacks was completed on-board. Zero traces were inserted for missing shots to account for <10 km wide gaps and jumps in the line geometry. Line gaps of >10 km were processed as separate lines (Fig. 2; Table S2). A 25 m CMP spacing ensured a good signal-to-noise (S/N) ratio. A standard final processing flow was used with GLOBE CLARITAS seismic processing package and included: resampling the data down to 2 ms, applying a 225–250 Hz low pass filter, standard muting of noisy traces and data spikes before velocity analyses, followed by stacking. After stacking, a band-pass filter of 4–24 Hz was applied, followed by finite difference migration with a maximum migration dip-angle of 45°, and 100% of the NMO velocities were used. The finite difference post-stack migration produced a clearer true-dip image. The velocity models were constrained by records from sonobuoys deployed along some profiles.

3.2. Interpretation approach

3.2.1. Type section

Prior to interpreting the relevant AWI-2010 and TAN-2006 lines (Table S2) or linking it with the interpretation of previous surveys, we identified the prominent horizons, unit, or sequence boundaries observed in the processed seismic images alone. To achieve this unbiased approach, we selected a representative type section in the central part of the Amundsen Sea basin on line AWI-20100110 (Figs. 1, 2). It was chosen at this basin-centre location, under the assumption that the sediments were likely to be the thickest and least disturbed, and would as such present the best possible opportunity to identify all the potential basin-wide units (Fig. 3; see Fig. 1 for location). In mapping the initial prominent first and second order sequence boundary horizons, we looked for variations in seismic facies characteristics such as reflectivity, reflection continuity and internal geometry (Fig. 3).

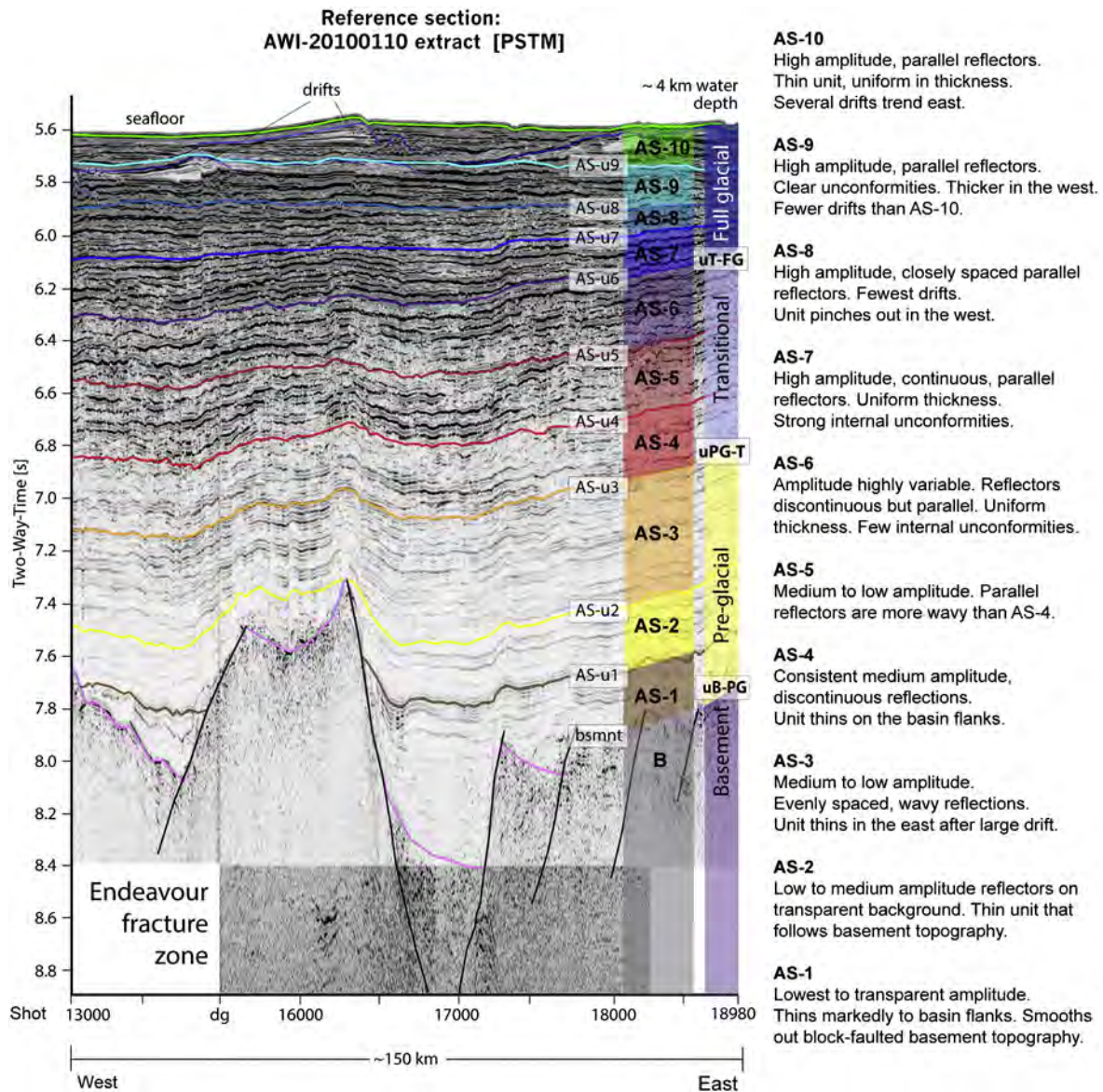


Fig. 3. Type section of the seismic reflection units AS-1 to AS-10, observed in the Amundsen Sea rise basin (Fig. 1 for location), with unit characteristics on the right. The units are separated by unconformities or boundaries of abrupt reflection characteristic change, labelled AS-u1 to AS-u10. The pre-glacial (PG), transitional (T) and full glacial (FG) regime sequences are separated by the base reflector discontinuities uB-PG, uPG-T and UT-FG, respectively. Black lines in the basement indicate block faulting associated with the Endeavour fracture zone (EFZ).

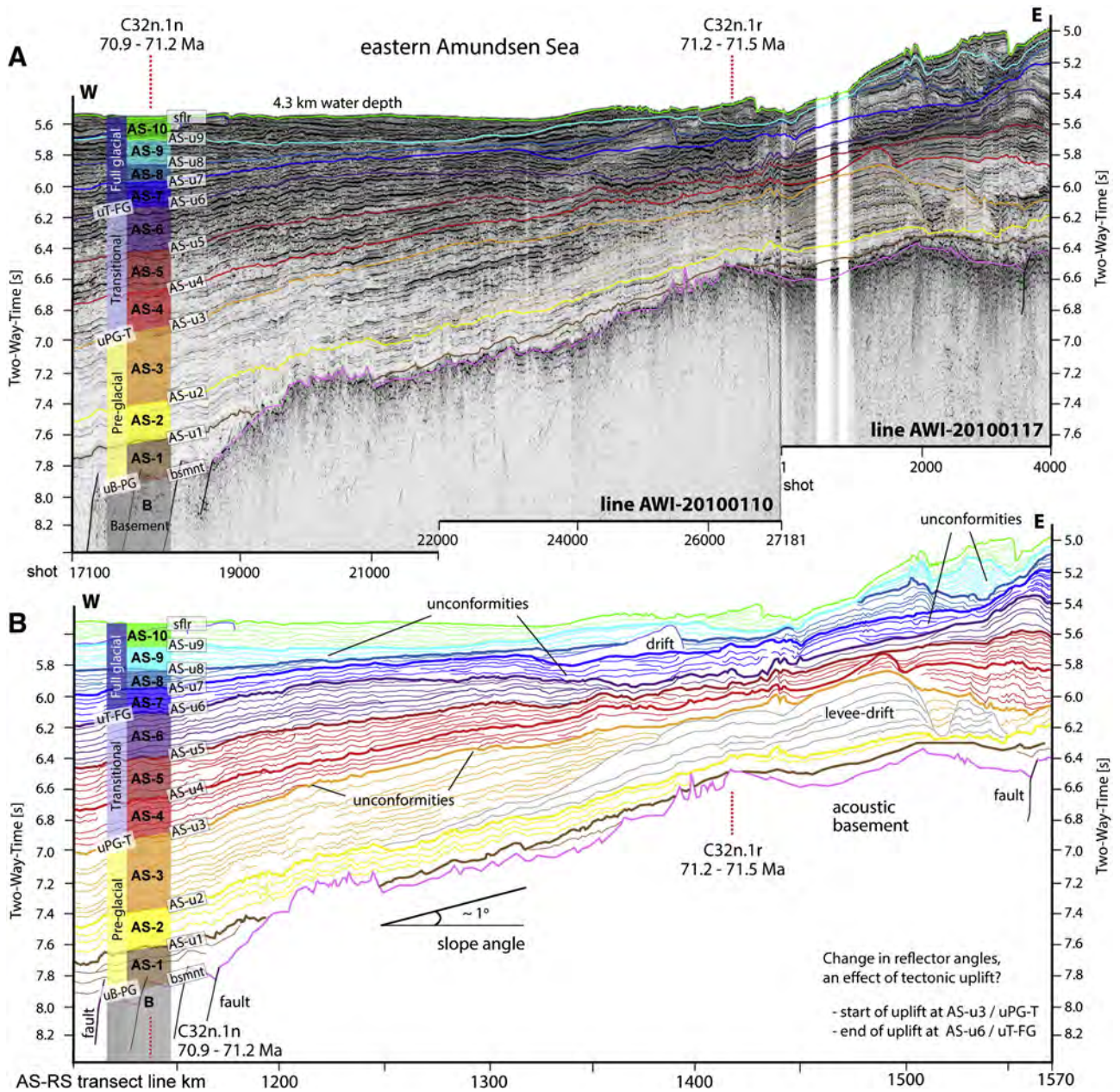


Fig. 5. (A) Segment of the central AS–RS transect with the main seismic units and boundaries, overlain and annotated. Red dashed lines represent the chrons of the oceanic basement. (B) Line drawing of the seismic image with the unconfomities annotated. Note the change of the reflector dip angles from bottom to top. A second order internal unconfomity occurs in AS-3, which terminates against the levee-drift.

3.2.2. Seismic characterisation

Subsequently, we compared our initial horizons in the type section interpretation (Fig. 3) to studies in other deep sea basins around Antarctica that used changes in seismic facies and internal geometry to identify pre-glacial to glacial sedimentary sequences in seismic reflection data, some of which are tied to drilling information (e.g. eastern Amundsen Sea: Nitsche et al., 1997, 2000; Uenzelmann-Neben and Gohl, 2012; Bellingshausen Sea: Scheuer et al., 2006; Weddell Sea:

Maldonado et al., 2006; Lindeque et al., 2013; Riiser Larsen Sea: Leitchenkov et al., 2008; Cosmonaut Sea: Leitchenkov et al., 2007a; Mawson Sea: Leitchenkov et al., 2007b; Wilkes Land: De Santis et al., 2003; Escutia et al., 2011; Ross Sea: De Santis et al., 1995; Brancolini and Leitchenkov, 2010). We used these collective interpretations and seismic horizon characteristics of the pre-glacial to glacial units as analogues to assess if similar packages and depositional processes apply to the AS–RS transect and relevant TAN-2006 lines. We base our

Fig. 4. Data and sequence-stratigraphic interpretation of the Amundsen Sea to Ross Sea transect. (A) Seamless seismic image of the western, central and eastern Amundsen Sea and eastern Ross Sea, represented as a time-migrated section. White strips in the seismic image signify data gaps. Interpreted horizons and units are identified according to the type section (Fig. 3). Red dashed lines represent the chrons of the oceanic basement (Fig. 2). Locations of Figs. 5 and 6 annotated. (B) Interpretative line drawing of the time-migrated seismic section. Note the presence of drifts in units AS-3 (east), AS-5 (west), AS-8 (east and west), AS-9 (west and central) and AS-10 (west and central) shown in light grey. Red squared and dashed drop down lines represent the 12 points selected for sediment thickness and sedimentation rate calculations (Fig. 10, Tables S3, S4; Fig. S2). (C) Seismic units represented as those deposited in the pre-glacial climate regime, the transitional climate regime, and full glacial climate regime. Each group is separated by a regional unconfomity, labelled uPG-T and uT-FG, respectively. (For interpretation of the references to colour in this figure legend, the reader is referred to the web version of this article.)

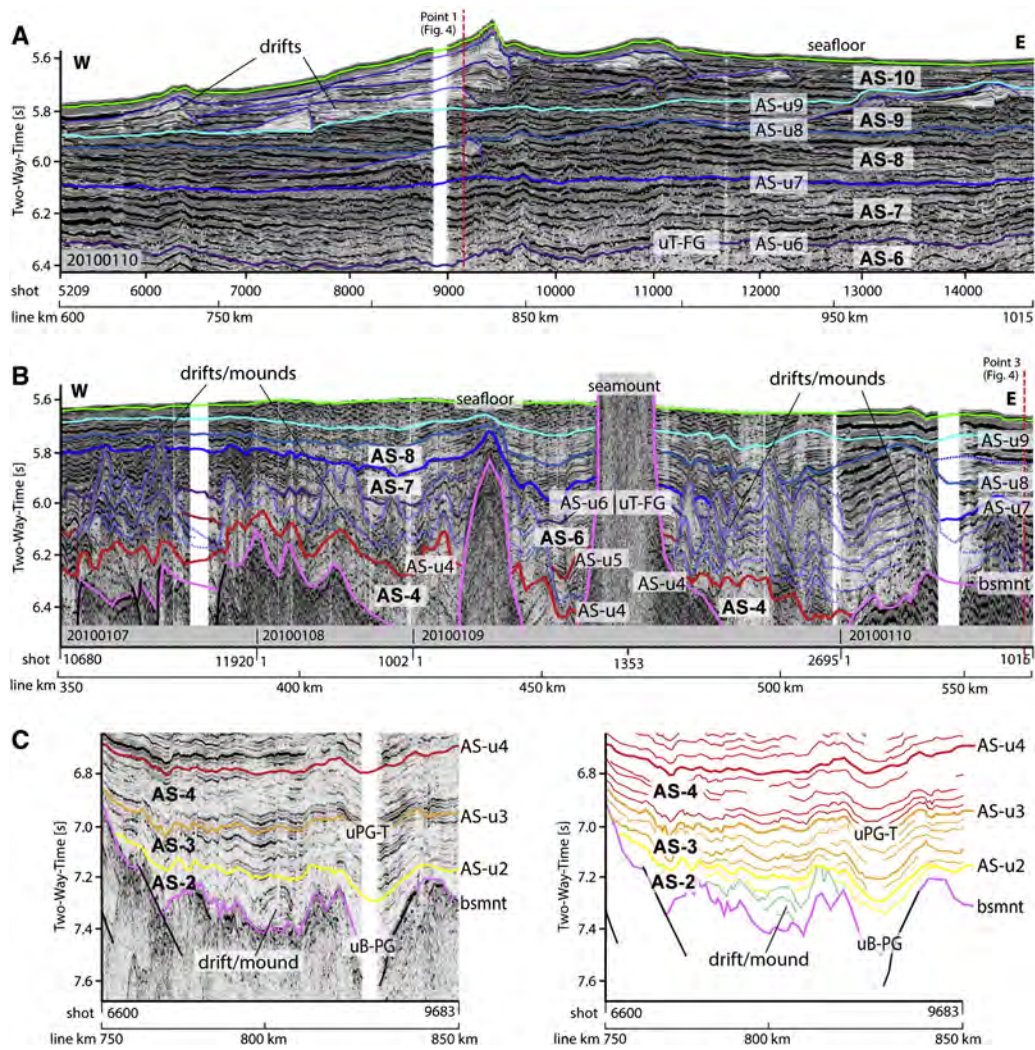


Fig. 6. Segments of the AS-RS transect highlighting the drifts or mounds observed in the pre-glacial, transitional and full glacial sequences. (A) Full-glacial sequences on line AWI-20100110. The number of drifts increases from one in AS-8, to two in AS-9, then to several stacked and more widely distributed ones in AS-10. The main base of the stacked drifts lies on AS-u9. (B) Composite segment of the transitional sequences of lines AWI-20100107 and AWI-20100110. The drifts or mounds, defined by the dashed lines, cut through units AS-5 and AS-6, as well across the transitional to full-glacial unconformity AS-u6/uT-FG, and even into the full-glacial unit AS-7. (C) Extracted pre-glacial sequences of line AWI-20100110 with seismic image on the left and line drawing on the right, illustrating the mound on the basement.

comparison on internal geometry such as drifts (i.e. mound shaped asymmetric ridges with internal strata pinching out on the steepest side of the mound) and channel-levees (i.e. mound shaped asymmetric ridges aggregated through repeated overspill events from the channel axis created by turbidity flows). The assumption is that if these sequences have already been identified on a circum-Antarctic scale in several of the deep-sea basins, two of these locations being on either side of the study area, it would be very likely that similar sequences could be present in the AS-RS transect and connecting lines.

In some parts of the eastern Amundsen Sea and around the Marie Byrd Seamounts the FG and T sequences contain distinctive mass sediment transport bodies, such as sheeted or mounded drifts, interpreted to have formed by contour and coast parallel bottom currents (e.g. Uenzelmann-Neben and Gohl, 2012). Hence identifying drifts in the seismic images of the AS-RS transect, could similarly provide an indication of the depositional processes and palaeo-bottom current activity in the central Amundsen Sea basin.

3.2.3. Horizon mapping

The type section interpretation (Fig. 3) was expanded into the regional basin context along our 2000 km long AS-RS transect (Fig. 1). The AS-RS transect was constructed from 8 profiles of continuous

seismic data from the AWI-2010 survey (Fig. 4a). To test the initial unit boundary horizons interpretation in the type section (Fig. 3) within the AS-RS transect, not only the marker horizons but also every internal reflection, were traced up to the farthest western and eastern flanks of the basin and for the full extent of the transect dataset. In doing so, we were able to identify low-angle onlap or downlap unconformities and depositional angle changes (Figs. 4b, 5; Fig. S1a, b). Lastly we mapped the basement, the corresponding fracture zones (Figs. 2, 4), and larger internal structures such as sediment drift bodies (Figs. 4b, 6; Fig. S1b). Independent analyses of the central transect placed us in a position to assess if the unit boundaries and preliminary sequence boundaries correlate with the existing interpretations in the Ross Sea and eastern Amundsen Sea (Fig. 1).

3.3. Integration with pre-existing seismic data

3.3.1. Seismic reflection surveys

There are three points where the AS-RS transect ties into the regional seismic survey network. The first is at the western end of the AS-RS transect, linking the Amundsen Sea seismic profile network with that of the eastern Ross Sea (Fig. 2). Lines AWI-20100107 and AWI-20100108 connect to line TAN-2006-06a, whereas line TAN-2006-06c

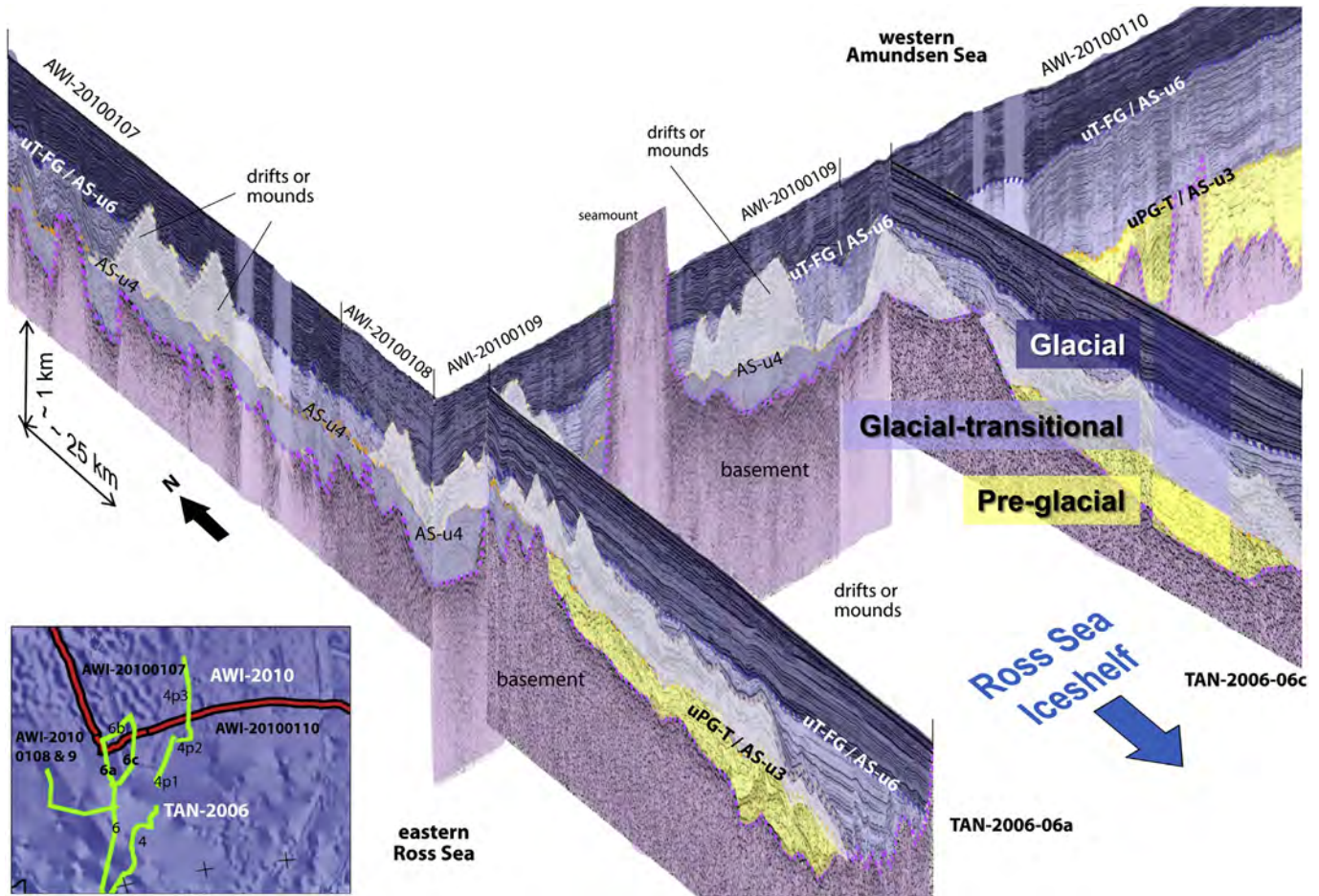


Fig. 7. 3D image illustrating the seismic stratigraphic link of the pre-glacial to glacial sequences between the TAN-2006 data in the eastern Ross Sea and the corresponding horizons interpreted on the AWI-2010 survey data in the western Amundsen Sea. The correlation of the pre-glacial to transitional unconformity uPG-T (AS-u3) and the transitional to full-glacial unconformity uT-FG (AS-u6) are annotated. Note the drifts or mounds, in pale grey, terminate on AS-u4 or the basement and cut into the full glacial sequence (dark blue polygon). These are especially visible in lines AWI-20100107 and TAN-2006-6a. Inset: Location of the lines used for the 3D link construction annotated in bold (see Fig. 1 for location in the larger study area). Thick red line with black border—the AS-RS transect (Fig. 4) comprising AWI-2010 seismic data, of which lines AWI-20100107, -108, -109 and a part of -110 were used in the 3D image, annotated. Green lines—the TAN-2006 seismic data, of which extracts of lines 6a and 6b were used, annotated. (For interpretation of the references to colour in this figure legend, the reader is referred to the web version of this article.)

crosses line AWI-20100109 (Figs. 1, 2, 7). Since the TAN-2006 dataset has no previously published interpretation, the AS-RS transect horizons were extended onto these lines.

The second key seismic stratigraphic link is the Ross Sea shelf-slope-rise connection between the AS-RS transect interpretation and the interpretation of the BGR80 seismic lines (Hinz and Block, 1985; ANTOSTRAT, 1995), in particular, line BGR80-005 connecting to TAN-2006-06 (Figs. 2, 8; Table S2). Line ATC82B-203 (Fig. 2; Wannesson et al., 1985) provided additional information on the shelf break where the reflections are obscured by multiples or unclear. The BGR80-005 interpretation was used as published (Hinz and Block, 1985; ANTOSTRAT, 1995). The AS-ux unconformities were traced up the slope, across the shelf along lines BGR80-003 and BGR80-004 (Fig. 2; Table S2) and to line PD-30, interpretation used as published (Anderson and Bartek, 1992).

The third key seismic stratigraphic link lies in the eastern Amundsen Sea, at the eastern end of the AS-RS transect (Figs. 1, 2). At this intersection, profile AWI-20100117 of the AS-RS transect crosses lines AWI-94050 and AWI-94054 (Fig. 9, Table S2; Gohl et al., 1997; Nitsche et al., 1997, 2000; Uenzelmann-Neben and Gohl, 2012), linked to line AWI-20060200 (Table S2; Uenzelmann-Neben and Gohl, 2012; Kalberg and Gohl, 2014) and to AWI-20060023, crossing the eastern Amundsen Sea drift deposits (Uenzelmann-Neben and Gohl, 2012, 2014). These lines connect farther east to profiles extending to the Bellingshausen

Sea (Nitsche et al., 1997, 2000; Scheuer et al., 2006). The AWI-94050 and AWI-94054 horizons and interpretations were used as published (Uenzelmann-Neben and Gohl, 2012) and match the proposed central Amundsen Sea basin horizons (Figs. 3, 4; Fig. S1). Line AWI-20060200 was newly interpreted, because a detailed seismic horizon interpretation is as yet unpublished.

3.3.2. Borehole information

Since boreholes are absent from the Amundsen Sea continental rise and shelves, we used the borehole controlled age model from the eastern Ross Sea outer shelf, derived from Deep Sea Drilling Project (DSDP) Leg 28 Sites 270–272 (Figs. 1, 2; Hayes et al., 1975; Bart, 2003). This age model serves as a guide to estimate the age ranges of the interpreted slope and deep-sea horizons in the AS-RS transect via a series of seamlessly linked profiles and extended horizons (Figs. 2, 4–9; Fig. S2; Table S2 and references therein).

DSDP Leg 28 Sites 273 and 274 have been correlated to the ANTOSTRAT seismic sequences (Brancolini et al., 1995) via a series of acquired and archive seismic reflection tie lines (Fig. 2 in Granot et al., 2010). Good data continuity in seismic lines BGR-001, 13 and 14 (Fig. 4 in Granot et al., 2010) ties the shelf-slope correlation of the mid-Miocene RSU4 unconformity to DSDP Leg 28 Site 273 located on the shelf (Figs. 1 and 2), but the shelf-slope correlation of the older, prominent unconformity RSU6 was not possible due to seafloor

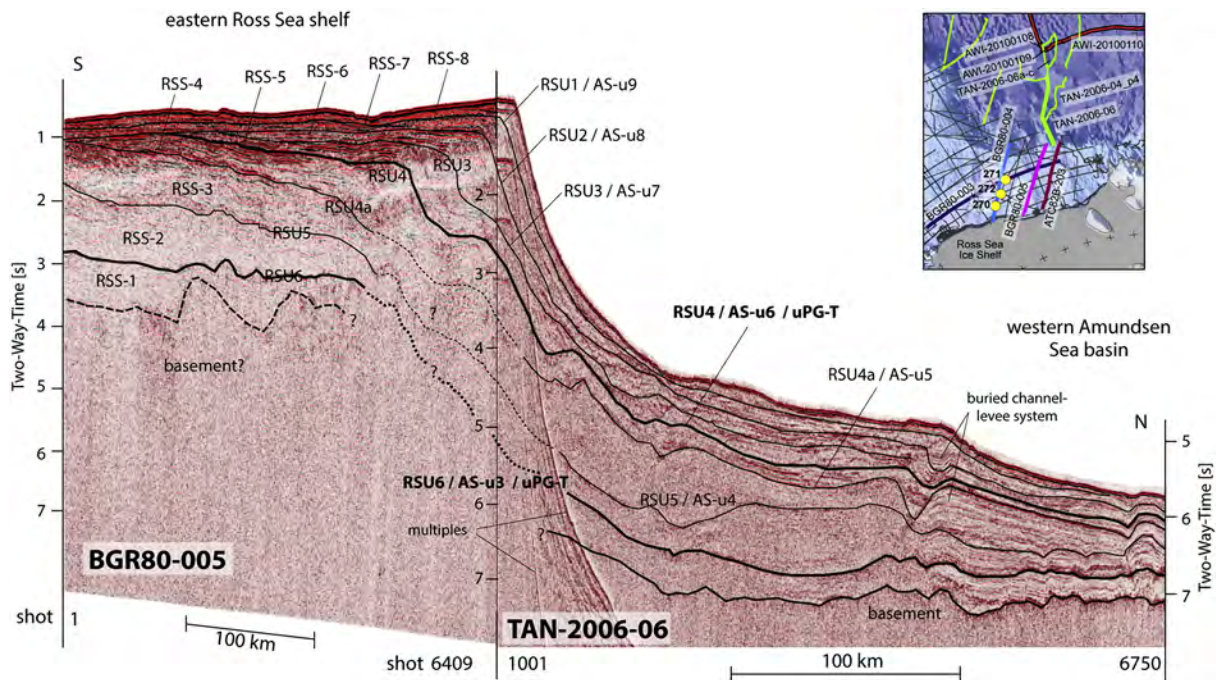


Fig. 8. Seismic line illustrating the shelf-slope-rise seismic stratigraphic link between the TAN-2006-06 line and BGR80-005 line in the eastern Ross Sea. The profiles are shown in an angled 3D-view (Geocap) and tilted so that the seabed aligns, and the white-space gap between the two lines (inset) closes. This is why the two TWT scales do not match as in a traditional 2D-view. The profiles are however correctly georeferenced. The middle vertical timescale line has been added-in for clarification. See Table S2 for the key references and acquisition parameters. Seismic line PD90-30 (Anderson and Bartek, 1992) and DSDP Leg sites 270, 271 and 272 (Fig. 1) (Hayes et al., 1975) have already been correlated to line BGR80-005 via a series of lines (Fig. 2). The line BGR80-005 stratigraphy was taken as published (Brancolini et al., 1995; Brancolini and Leitchenkov, 2010) and in the absence of slope drilling information, correlated to the TAN-2006-06 line and AWI-2010 AS-RS transect. Inset: Location of the lines used for the 3D link construction, same as for Figs. 1 and 2. Refer to the uninterpreted image in online supplement Fig. S3.

multiples. Line 9 however, ties the Eocene/Oligocene transition RSU6 unconformity to DSDP Leg 28 Site 274 (near shot point 450, Fig. 5 in Granot et al., 2010). Since DSDP Leg 28 Site 274 is located on the lower slope/continental rise and the seismic facies characteristics of their deeper lines (e.g. line 4a, shot point 8500 – 9000, Fig. 10 in Granot et al., 2010) appear similar to those observed in the AS-RS transect, we also used the Granot et al. (2010) chrono-stratigraphic model as a guide for our interpretation.

The nearest other relevant deep borehole on the continental rise, International Ocean Drilling Program (IODP) Leg 318, Site U1356 lies off the Wilkes Land margin, approximately 1300 km to the west of the most western end of our AS-RS transect (Fig. 2 inset; Escutia et al., 2011). We used the seismic reflectivity characteristics of the dated and biostratigraphically analysed pre-glacial, transitional and full-glacial sequences as an analogue to place observations of the AS-RS transect in a provisional chrono-stratigraphic framework.

To the east of the Amundsen Sea, the nearest borehole DSDP Leg 35 Site 324 (e.g. Tucholke et al., 1976) is located in the Bellingshausen Sea, about 1000 km from the eastern end of the AS-RS transect (Fig. 2). This site only provides information for the uppermost 200 m Pleistocene and Pliocene sediments. DSDP Leg 35 Site 323 lies on the abyssal plain and contains predominantly pelagic deposits. Neither of these two drill sites was considered useful for the objectives of this work.

Farther to the east on the Antarctic Peninsula margin, Ocean Drilling Project (ODP) Leg 178 Site 1095 is more applicable (Fig. 2 inset; Barker et al., 2002). Sequences of mid-Miocene age in a sediment drift deposit were drilled, dated and mapped (e.g. Iwai et al., 2002; Uenzelmann-Neben, 2006). Although the drill site lies more than 2000 km from the eastern end of our AS-RS transect, it was used in Scheuer et al. (2006) and Uenzelmann-Neben and Gohl (2012) for the horizon correlation and age model verification in the Bellingshausen Sea (Figs. 1, 2), and is therefore considered as supporting information for the interpretation of our transect.

3.3.3. Seismic velocity measurements for sediment thickness estimates

Sediment thickness and depth sections were constructed from 12 points along the AS-RS seismic transect (Figs. 1, 4; Figs. S1, S2). The points were chosen to represent trends of changes in sediment thickness and basin geometry and are therefore irregularly spaced. Due to distant borehole information and absent seismic refraction data in the central Amundsen Sea basin, we depended on interval velocities derived from RMS stacking velocities for time-to-depth conversions (Fig. S2; Table S3). Supporting velocity information was extracted from sonobuoys 5 and 8 collected on the eastern Ross Sea rise during the TAN-2006 expedition (Fig. 2) and compared to a seismic refraction model from ocean-bottom seismometer (OBS) data along profile AWI-20060200 east of the AS-RS transect (Fig. 2; Kalberg and Gohl, 2014). The interval velocities used are consistent with the sonobuoy velocities and compare well to the refraction velocities.

3.4. Age model and sedimentation rate estimates

Oceanic basement age control of the central Amundsen Sea was obtained from the magnetic seafloor spreading anomalies of Wobbe et al. (2012; Fig. 2). The top-of-basement reflection in each of the 12 points used in the sediment thickness and depth sections (Fig. 4; Fig. S1), were assigned the age of the closest isochron, or the age was linearly interpolated between the two closest magnetic spreading anomalies. This age was then used to place the basement horizon in each of the 12 sections at the corresponding age position on the geological time scale, and the sections vertically stretched so that seafloor matched present time (Fig. 10). The first and last occurrence of each sequence, across all 12 points, were projected back onto the time scale in order to estimate the relative depositional time span (thin colour bars on the left in Fig. 10). The deduced age range for each sequence was subsequently used in conjunction

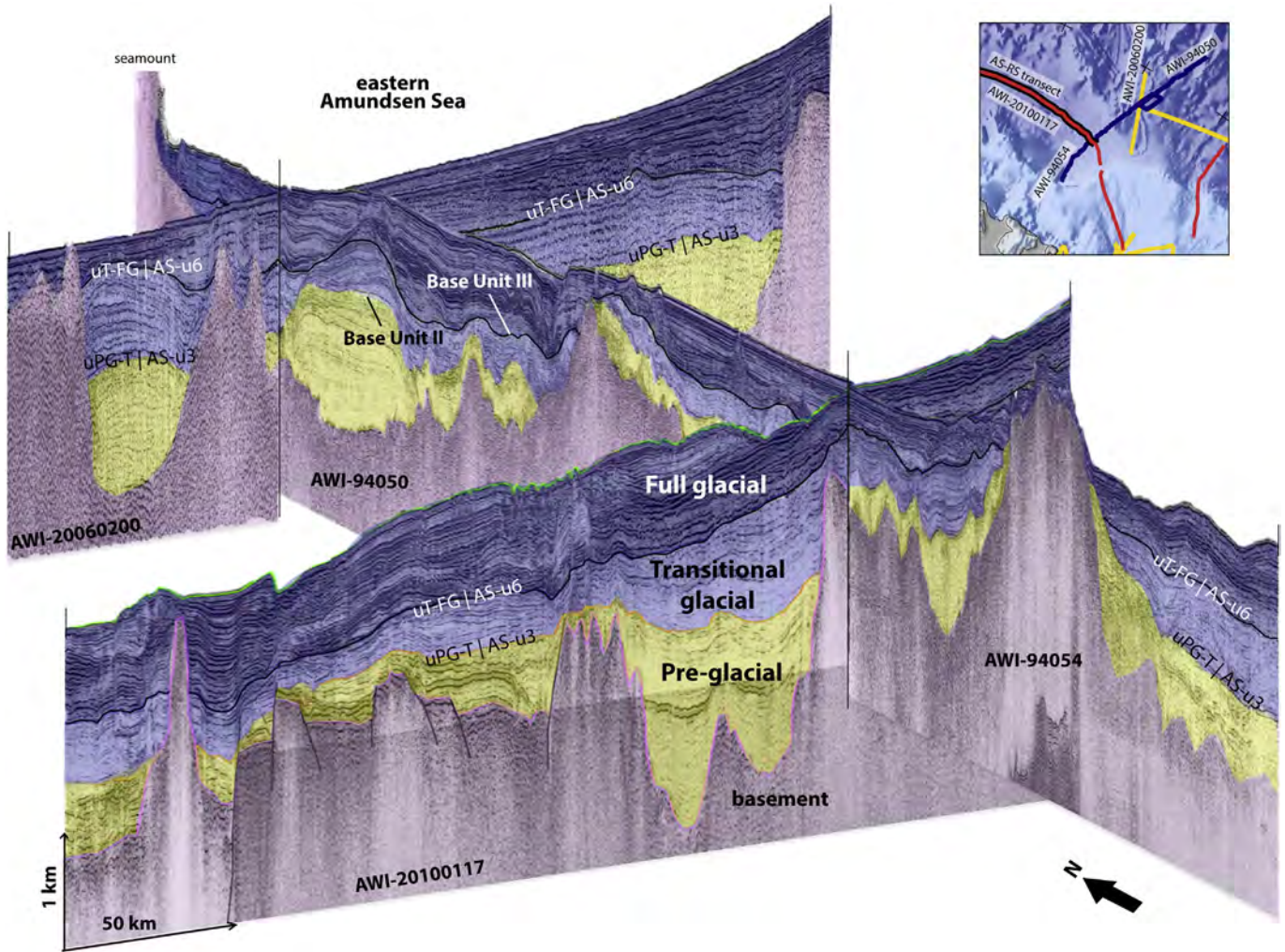


Fig. 9. 3D image illustrating the seismic stratigraphic link of the pre-glacial to glacial sequences in the eastern Amundsen Sea. Sequence boundaries interpreted in the AS-RS transect were correlated to the corresponding horizons in lines AWI-94050, AWI-94054 (Uenzelmann-Neben and Gohl, 2012) and AWI-20060200 newly interpreted. The two main sequence boundaries, uPG-T (AS-u3) and uT-FG (AS-u6), align with the bases of Unit II and Unit III, respectively. Inset: Map showing location of the lines used for the 3D link construction. Refer to Fig. 1 for the location in context of the larger study area.

with the 12 point-based sediment thickness estimates (Fig. S2; Table S3) to calculate the sedimentation rates (Table S4).

4. Results

4.1. Seismic interpretation and horizon characteristics

4.1.1. Type section and nomenclature definition

Prominent horizons or unconformities were assigned up-sequence as AS-u1, AS-u2 etc., where AS stands for Amundsen Sea and -ux for the unconformity number. Similarly, units between two boundary horizons were assigned AS-1, AS-2 etc. and numbered up-sequence (Figs. 3, 4 and Fig. S1).

We started the interpretation with the delineation of the crystalline basement horizon and observed faulting in the type section (Fig. 3). Continuing up from the top of basement, the first high amplitude, continuous reflection was assigned as AS-u1, followed by AS-u2. Both reflectors stood out prominently against the low amplitude to transparent background. The next unit transitions were identified at reflections AS-u3, AS-u4, and AS-u5, as amplitudes increased consistently up-sequence, and the internal unit reflection geometry changed to become progressively more closely spaced (Fig. 5; Fig. S1). AS-u6 is mapped along a low angle unconformity with onlap up-dip (6.2–6.4 s and shot numbers 17000–18000 in Fig. 3; Fig. S1) and also marks a strong

amplitude increase of all the units above this horizon. AS-u7 and AS-u8 are high-amplitude unconformities as well, and -u9 was chosen at the base of sediment drifts, but above what seems to be a truncated drift (at 5.75 s and shot numbers 15000–16500 in Figs. 3, 4 and Fig. S1).

To identify the pre-glacial to glacial sequences and characteristics, we compared our type section to other type sections of deep-sea basins around Antarctica. These studies typically describe the pre-glacial (PG) seismic sequences as the initial series of discontinuous reflections from low amplitudes to transparent reflectivity, occurring just above the basement. Internal reflections are predominantly parallel to each other and the basement topography. If plotted without filtering the display, this sequence appears light grey to white on a greyscale seismic image e.g. units below WL-u3 in Escutia et al. (2011), unit WL-S3 in De Santis et al. (2003), Unit I in Uenzelmann-Neben and Gohl (2012) and units WS-S1 to WS-S3 in Lindeque et al. (2013). The reflections in the transitional (T) units have been described as closer spaced, horizontal to wavy, with internal structure or discontinuities and of medium amplitude. Buried drifts and cut-and-fill geometries can occur infrequently. This sequence typically has a medium grey appearance if plotted without display filter adjustments, e.g. WL-S4 and WL-S5 in Escutia et al. (2011) and De Santis et al. (2003), Unit II in Uenzelmann-Neben and Gohl (2012; Fig. 9) and unit WS-S4 in Lindeque et al. (2013). The full glacial (FG) sequences were mostly characterised by the highest amplitude reflections and strong lateral continuity. Internal reflections

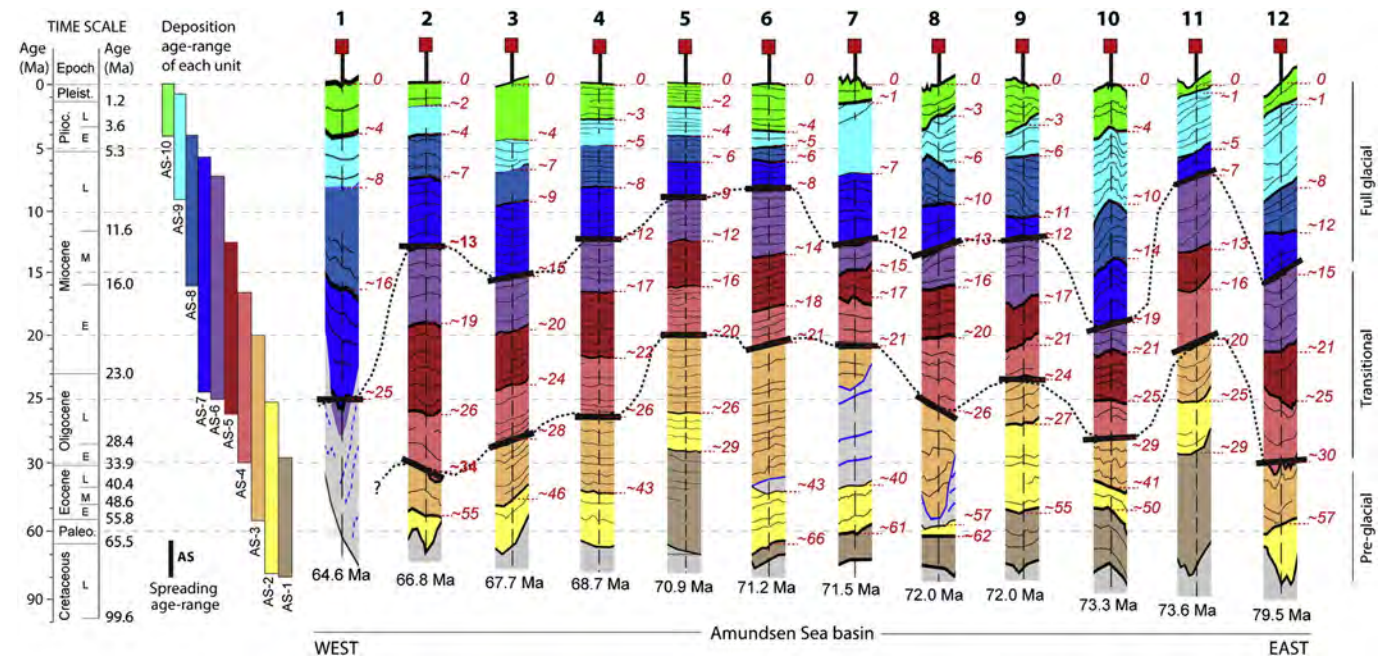


Fig. 10. Age model and associated deposition along the AS-RS transect. From left to right: Time scale of epochs and boundary ages after Gradstein and Ogg (2004), L—Late, M—Middle, E—Early. Narrow colour bars—first and last occurrence of each unit, projected onto the time scale. Broader colour columns – interpreted horizons, extracted from the 12 points along the AS-RS transect and represented as a section scaled to time (Figs. 1, 4; Figs. S1, S2). Black dashed lines and bars depict the interpreted top and bottom boundaries of the transitional sequence. Red italic numbers represent the tentative age estimate (in Ma) for each horizon. The black numbers below each column are the estimated basement ages at each point, taken from the magnetic seafloor anomalies in Fig. 2. (For interpretation of the references to colour in this figure legend, the reader is referred to the web version of this article.)

are parallel and very closely spaced, with a collective dark grey to partly black appearance on a greyscale seismic image without display filters e.g. WL-S6 to WL-S8 in Escutia et al. (2011) and De Santis et al. (2003), Units III and IV in Uenzelmann-Neben and Gohl (2012; Fig. 9) and unit WS-S5 to WS-S7 in Lindeque et al. (2013).

Using the seismic characteristics identified in these other studies as a guide, we visually identified the uPG-T and uT-FG boundaries in our type section, interpreted as separating the 1st order pre-glacial, transitional and full-glacial sequences (annotated in Fig. 3). In our central Amundsen Sea type section (Fig. 3), we describe the pre-glacial, transitional and full glacial sequences as follows:

The pre-glacial, PG sequence, displays a low to transparent reflectivity and lack of internal structure, which indicates well-sorted sediments and relatively uniform sedimentation processes over long times, probably associated with the greenhouse period of Antarctica.

The transitional, T sequence, has medium to low amplitude reflectivity and reflections are discontinuous, parallel and evenly spaced. The higher amplitudes are probably due to the interlayering of strata with different grain sizes (e.g. turbidites) or alternation of well and poor sorted sediment strata (e.g. diamictites-debris flows and hemipelagites) associated with increased down-slope gravity-driven, and along-slope bottom current driven sediment transport processes. It is important to note that these interlayering sequences are widely distributed along the AS-RS transect, which discounts the possibility that they could be point sources causing diffractions.

The full glacial, FG sequence, shows the highest continuous reflectivity and the reflections are parallel and very closely spaced. Drifts occur in units AS-9 and AS-10. These deposits are interpreted as being indicative of the continued supply of predominantly poorly sorted material through mass down-slope sediment transport processes as grounded ice sheets repeatedly advanced across the shelf, followed by redistribution along the continental rise by strong bottom-current activity. Sediment drift building by contourite currents is a major characteristic observed for the FG phase (e.g. Uenzelmann-Neben, 2006; Rebesco et al., 2014; Figs. 4–6; Fig. S1).

Although these type sections in the Weddell Sea, eastern Amundsen Sea and Wilkes Land studies sections are far apart from each other, and from this study's central Amundsen Sea type section, the visual resemblances of the PG, T and FG sequences between the type sections are striking when placed directly next to each other.

4.1.2. Seismic characterisation and horizon stratigraphy

We used the nomenclature and marker horizons from our type section (Fig. 3) to map the remaining full length of the AS-RS transect and present new basin-wide seismic stratigraphy for the Amundsen Sea deep-sea basin (Figs. 4, 5; Fig. S1).

The acoustic basement topography is irregular and rugged along the western basin flank (line AWI-20100107) as well as on the eastern Amundsen Sea flank (line AWI-20100117). The basin geometry deepens towards middle of the transect, forming a classic 'saucer shape' and a valley in the centre (line km 1000 to 1200 in Fig. 4; Fig. S1). To the west of the centre point (line km 700 to 1100), typical block faulting was mapped. The fracture zones predicted in the magnetic data (Wobbe et al., 2012) match major basement faults observed in the AS-RS transect (Kohiko-, Pahemo- and Endeavour FZs in Fig. 4; Fig. S1). In the region east of the centre point (line km 1100 to ~1650) and up to the first seamount (line km 1700 in Figs. 4, 5), the basement topography is smoother and without faulting. The slope angle of this anomalous part is ~1° (Fig. 5).

The seismic reflectivity characteristics of units AS-1 to AS-10 in the AS-RS transect (Fig. 4; Fig. S1) match the characteristics for each unit described in the type section (Fig. 3) well and lateral variation is negligible. Marker horizons AS-u1 to AS-u9 are laterally continuous and easy to trace along the ~2000 km AS-RS transect distance. Every internal reflection was mapped over the full transect length and low-angle unconformities and onlaps or downlaps identified, which increased confidence in deciding on the PG, T and FG sequence boundary horizons (Figs. 4b, 5b; Fig. S1b).

In general, the horizons are mostly parallel to the general basin geometry and top-of-basement trend, except above the anomalous

Wilkes Land Basin		Ross Sea shelf and slope			central Amundsen Sea basin			far eastern Amundsen Sea basin			
Escutia et al., 2011		De Santis et al., 1999	Brancolini et al., 1995	Brancolini & Leitchenkov 2010	This study			Uenzelmann-Neben 2006; Uenzelmann-Neben and Gohl 2012	Nitsche et al. (1997, 2000)		
seafloor		seafloor			west	central	east	seafloor			
WL-S9	RSU1	RSS-8	2.5	1.5 Ma	AS-u9	~2 Ma	AS-10	~2	~1 Ma	Unit IV	
WL-S8	RSU2	RSS-7	4.0	3.3 Ma	AS-u8	~4 Ma	AS-9	~5	~8 Ma	4 Ma	Unit 1
WL-S7	RSU3	RSS-6	10.5	10.5	AS-u7	~9 Ma	AS-8	~6	~12 Ma		Unit III
WL-S6	RSU4	RSS-5	16.5	14.7	AS-u6	~15 Ma	AS-7	~9	~15 Ma	14 Ma	
WL-U5	RSU4a	RSS-4	17.0	18.5	AS-u5	~20 Ma	AS-6	~14	~21 Ma		Unit II
WL-U4	RSU5	RSS-3	21.0	30-22	AS-u4	~26 Ma	AS-5	~18	~25 Ma		Unit 2
WL-S4	RSU6	RSS-2	30.0	34-30	AS-u3	~34 Ma	AS-4	~21	~30 Ma	21 Ma	
WL-U3					AS-u2	~55 Ma	AS-3	~43	~57 Ma		Unit I
					AS-u1	~66 Ma	AS-2	~66	~80 Ma		Unit 3
basement		RSS-1 volcanics			bsmnt	~67 Ma	AS-1	~71	~80 Ma	60 Ma	
		basement					basement			basement	basement

Fig. 11. Seismic stratigraphy correlation chart that illustrates the links of the boundary horizons and the seismic units in this work, to previous studies of the Ross Sea shelf and eastern Amundsen Sea basin. Thick black lines—lower boundary of the proposed full glacial and transitional units; red numbers—ages of the horizons, showing the lateral variation across the basin from west to east. (For interpretation of the references to colour in this figure legend, the reader is referred to the web version of this article.)

part of the basin (line km 1100 to ~1650). This part was mapped in greater detail (Fig. 5). Up to AS-u3, the reflections are parallel to the basement slope trend and the internal unit reflections onlap against a drift and channel–levee structure in AS-3 (Figs. 4, 5; Fig. S1). A prominent reflection in the middle of AS-3 (6.4–6.8 s, shot 20000–25000 in Fig. 5) pinches out up-dip against the large sedimentary drift body and is laterally discontinuous. It was therefore interpreted as a sub-unit within AS-3.

Above AS-u3, the reflections become increasingly angular compared to the reflections below AS-u3, for example, the thinner red lines in unit AS-4 and AS-5 (Figs. 4b, 5b; Fig. S1). The internal unconformities are at their largest internal angles up to AS-u6; this is especially visible in the internal geometry of unit AS-6. Above AS-u6, the horizons trend changes to progressively more horizontal and parallel towards the top units, with complex internal geometry in the youngest unit, AS-u10 (Fig. 5b, between seafloor (sflr) and AS-u9; Fig. S1b).

After mapping all the marker horizons and every internal reflection, more low angle unconformities were noticed, which confirmed the initial marker horizon decisions chosen in the type section interpretation (Sections 4.1.1 and 3.2.1). It also cleared up the earlier ambiguity around AS-u3 (see unconformities in Fig. 5b onlapping against AS-u3; Fig. S1a,b).

The resulting PG sequence, units AS-1, AS-2 and AS-3, are bound by the basement reflection (bsmnt) below and the AS-u3 discontinuity above (Figs. 4, 5). AS-u3 or uPG-T was picked as the top boundary of this 1st order PG sequence, because it marks a change in seismic facies from low amplitude and more transparent reflections below, to higher amplitude reflections above. This gradational change is consistent with the descriptions of the pre-glacial to transitional unit progression seen in type sections in the other Antarctic margin basins (Section 3.2.2). AS-u3 also marks a change in the reflector angles (Fig. 5) and is demarcated from the low amplitude and different internal geometry units below by clear unconformities (Figs. 4b, 5b; Fig. S1b). The decrease

in amplitude in the deeper section can be due to acoustic energy loss, or due to the sediment type such as fine and homogeneous sediments deposited in a distal sector or sediments from a different source area.

The T sequence comprises units AS-4, AS-5 and AS-6 (Figs. 3, 4, 5). AS-u6 was picked as the top boundary of this 1st order T sequence because it marks a sharp change into the highest amplitude, finely layered reflective package above (Fig. 4a). Again, this is consistent with the descriptions of the pre-glacial to transitional unit progression, seen in type sections of the other Antarctic margin deep-sea basins. In addition, this horizon is a pronounced unconformable high amplitude reflector with reflections terminating against it and it delineates a prominent change in the reflection dip angles on either side (Fig. 5), which collectively may also indicate a tectonic uplift change. We interpret this sequence and associated seismic characteristics to indicate a rapid increase in the supply of large volumes of poorly sorted sediments, pushed across the shelf and spilled down the slope and into the abyssal plain, in a response to the first ice sheet advancements onto the shelf.

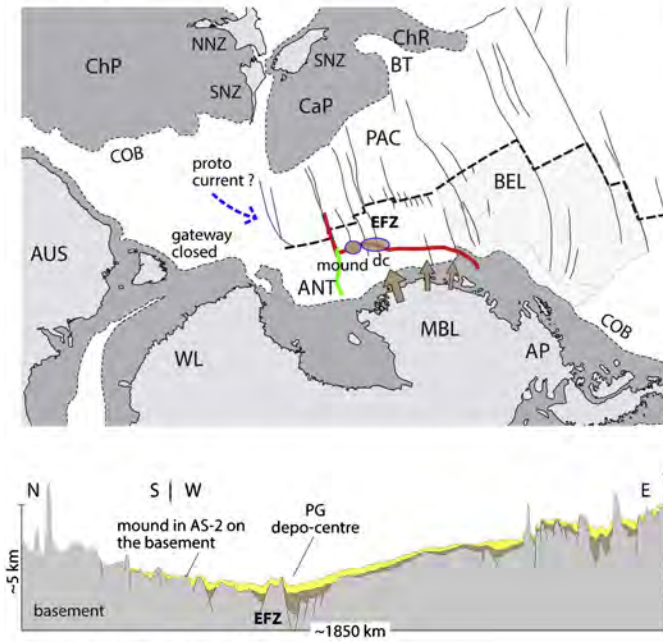
The FG sequence includes units AS-7, AS-8, AS-9 and AS-10. These units show more complex internal second and third order unconformities towards the top, and several internal drift structures (Figs. 3–6; Fig. S1). Increased occurrence of the complex internal drift structures represents changes in the depositional processes and bottom water circulation. This is consistent with the interpretations of Uenzelmann-Neben and Gohl (2012) in the adjacent eastern Amundsen Sea rise basin. The sharp transition at AS-u6 is interpreted to mark the onset of the full glacial polar climate regime and the establishment of a modern oscillatory polar ice sheet, consistent with drilling information from the IODP Leg 318, Site U1356 off the Wilkes Land margin (Escutia et al., 2011; Fig. 2 inset).

4.1.3. Drifts

Distinct sediment bodies are observed in the AS–RS transect (grey wedge-shaped structures in Figs. 4–6; Fig. S1) There are too many

A. CRETACEOUS - PALEOCENE

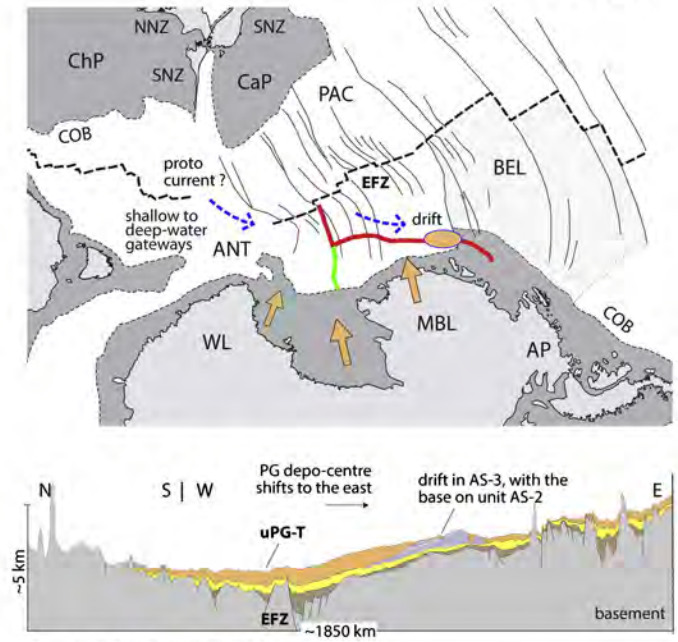
55.8 Ma



Pre-glacial regime units: AS-1, AS-2

B. EOCENE - OLIGOCENE

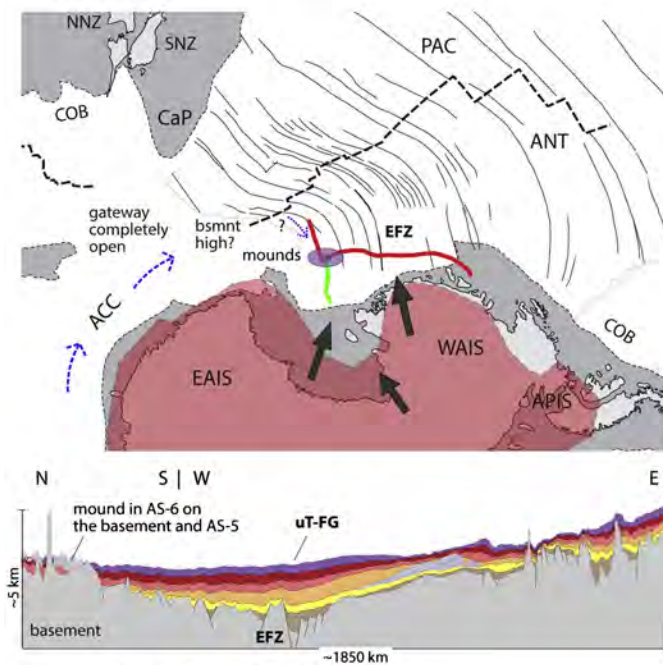
34.0 Ma



Pre-glacial regime units: AS-1, AS-2, AS-3

C. MID-MIOCENE

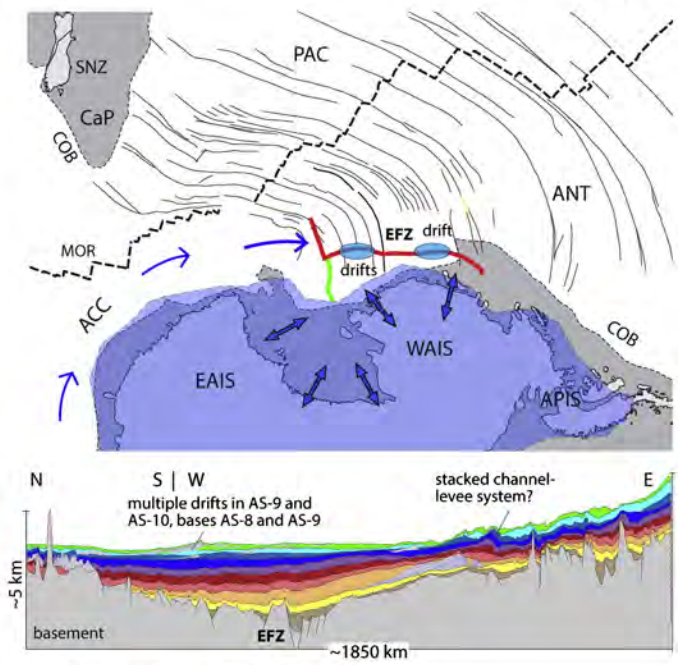
15.5 Ma



Transitional regime units: AS-4, AS-5, AS-6

D. PLIOC. - PLEIST.

4.8 Ma



Full glacial regime units: AS-7, AS-8, AS-9, AS-10

Fig. 12. Model showing the changes in plate-tectonic motion, pre-glacial to glacial sediment deposition, ice sheet development and ocean circulation in the Southern Pacific, and greater Amundsen Sea region since the Paleocene. The corresponding sediment deposition for each regime is illustrated in the AS–RS transect diagram below. Plate rotation adapted from [Wobbe et al. \(2012\)](#). Thick dashed black lines—MOR—mid-oceanic ridge, black lines—fracture zones, EFZ—Endeavour Fracture Zone, PAC—Pacific Plate, ANT—Antarctic Plate, BEL—Bellingshausen Plate, COB—continent–ocean boundary. The AS–RS transect is shown as a red line, linked with the TAN-2006-06 seismic profile (green line). Observed sedimentary drifts and mounds are indicated by ovals, and the arrows depict the inferred sediment supply and ocean circulation. Red and blue polygons illustrate the schematic extent of the East Antarctic Ice sheet (EAIS), West Antarctic Ice sheet (WAIS) and Antarctic Peninsula Ice sheet (APIS) expanding to the continental shelf during the transitional and full-glacial regimes. ChP—Challenger Plateau, ChR—Chatham Rise, CaP—Campbell Plateau, BT—Bounty Trough, NNZ—North Island of New Zealand, SNZ—South Island, AUS—Australia, WL—Wilkes Land, MBL—Mary Byrd Land, AP—Antarctic Peninsula. (For interpretation of the references to colour in this figure legend, the reader is referred to the web version of this article.)

mounds, drifts and channel–levees to show high-resolution images of their internal geometry or to give a detailed interpretation of each one. This would by far exceed the scope and size of the paper, and were purposefully left for future work. Here, only the main ones are briefly described in the context of the units within which they occur.

The PG sequence contains two sedimentary bodies. The first feature is interpreted as a buried giant channel–levee system on the eastern flank of the basin, indicative of large turbidite flows possibly related to glacial conditions on land (Escutia et al., 2000). However, such detailed classifications remain ambiguous in this case as the features are only imaged with a single 2D profile. The giant channel–levee system occurs near the basement and within the older pre-glacial unit AS-3, with its base on AS-2 (Fig. 5). It is ~3000 m long and almost 400 m high at the highest point (5.9–6.3 s TWT at line km 1475 in Fig. 5 and Fig. S1). The internal seismic reflections are distinct and continuous, forming a parallel lamination that follows the overall drift geomorphology, shown in more detail in Fig. 5b. The stoss side pinches out to the west.

The second PG sedimentary body is a smaller, approximately 80 km wide mound or drift, just to the west of the basin centre near the Pahemo FZ (line km 750 in Fig. 4b). It lies directly on the 68–65 Ma basement and is constrained to AS-2 (Fig. 6c, line AWI-20100110, shot 6604–9683). This feature is interpreted as a mound or drift, since it appears internally stratified. It could also be interpreted as a slope-slide block, or gas-fluid intrusion that folded overlying sediments. However, the resolution of this feature is limited and it is difficult to observe the actual internal stratification geometry; hence this single line only allows for an ambiguous or non-unique interpretation.

Smaller drifts or mounds occur in the T sequence and are concentrated on the western flank of the basin (profiles AWI-20100107, -108 and -109 in Figs. 4b, 6b; Fig. S1b). The base seems amalgamated and terminates on AS-u4, but the eastern part of the base lies directly on the 63–65 Ma basement (Fig. 6b, line km 520 onwards, in line AWI-20100110). The tops extend into units AS-5, AS-6 and AS-7 (line km 350 – 550 in Figs. 4b, 6b; Fig. S1b). The height is estimated as 400–500 m (Fig. 6b, 6.3–5.8 s TWT).

Fig. 6a illustrates an extract of the elongate sediment bodies observed in the FG sequence in line AWI-20100110 (shot 5209–14075 or CMP 7481–19312; Fig. 4). The number of drifts increases from one in AS-8 to two in AS-9, and to several stacked, more widely distributed ones in AS-10 (e.g. at shot 9000 and 5.6–5.9 s TWT; Fig. 6a; Fig. S1b). The main base of the stacked drifts lies on unconformity AS-u9. These drifts are typically 50–100 km wide and 200–300 m high, and occur in the central and western parts of the basin. They are usually confined to their respective seismic unit and may fill up part, or all of the unit thickness (Fig. 6a). The stoss side of all the drifts trend west. An additional feature interpreted as a stacked buried channel–levee system, can be seen in all the units to the east of the large PG sequence channel–levee system or drift (line km 1500 to 1600, Fig. 4).

4.2. Seismic stratigraphic links

4.2.1. Ross Sea rise link

The TAN-2006 and AWI-2010 surveys link seamlessly (Figs. 7, 11) and the horizons from the AS–RS transect were extended into lines TAN-2006-06, -06a,b,c, -04, 04p1, -p2 and -p4 in the Ross Sea (Table S2; Figs. 2, 7 inset, 11). Both lines TAN-2006-06a and -06c show drifts or mounds in their T units as well, and these tie with the mounds seen in lines AWI-20100108 and -109 (Fig. 7). The PG sequence (Fig. 7) pinches out against a basement high in the eastern Ross Sea (see bathymetry image in Fig. 1).

4.2.2. Ross Sea shelf-slope-rise link

The Ross Sea shelf seismic lines ATC82B-203 and BGR80-005 are nearest to line TAN-2006-06 (Figs. 2, 8 inset). The stratigraphy of the Ross Shelf was taken as published from Brancolini et al. (1995, 2010) and the link to line PD90-30 taken from Anderson and Bartek (1992).

The interpretation of DSDP Leg Sites 270, 271 and 272 (Hayes et al., 1975; Bart, 2003) via BGR80-003 and -004 was adopted as is (Figs. 2, 8).

Most of the AS-ux horizons on the TAN-2006-06 line could be traced and linked to parts of the interpreted Ross Sea shelf horizons, apart from a few slumping structures on the continental slope (Figs. 8, 11). As the shelf sequences are different from the deep-sea sequences in composition and depositional processes, we deemed only the age and nomenclature correlation of the horizons of relevance. Seafloor multiples in seismic records from the shelf made some of the correlation ambiguous, but nearby line ATC82B-203 provided useful additional information so that we are fairly confident on the correlation.

The AS-u1 reflector inside the PG sequence may have a similar strong reflectivity character as RSU6 in the eastern Amundsen Sea part of the AS–RS transect, interpreted as the top of volcanics and of Eocene age (Brancolini et al., 1995; Brancolini and Leitchenkov, 2010; Wilson et al., 2013). AS-u1, however, does not display the same ‘volcanic’ reflectivity character throughout. In the centre of the basin near the Endeavour fracture zone, the AS-1 seismic facies character rather suggests a sedimentary unit. AS-u1 and AS-u2 are not observed on the TAN-2006-06 line or western part of the AS–RS transect, but AS-u3 is. AS-u3 is also observed for the length of the AS–RS transect, into the eastern Amundsen Sea. Based on this regional continuation and consistent, strong prominent reflector characteristics (see detailed line drawing of each reflector and related discontinuities in Fig. S1b), AS-u3 rather than AS-u1 or AS-u2, is interpreted to represent the margin wide onset of glaciation process in this deep sea basin.

The horizon RSU6 is interpreted to be comparable to the AS-u3/uPG-T sequence boundary, and RSU4 to the AS-u6/uPG-T sequence boundary (Figs. 8, 11). Shelf horizon RSU4a appears to correlate with horizon AS-u5. This discontinuity is considered to be part of the transitional sequence as opposed to a first-order sequence boundary, since it terminates against AS-u6 (Figs. 5, 8 and Fig. S1). The suggested correlations of the other RSUx to AS-x horizons are annotated in Fig. 8. We use this slope–shelf interpretation to support our proposed chrono-stratigraphic model for the entire AS–RS transect, because it is currently the best available link to an age-controlled stratigraphy for the entire Ross Sea–Amundsen Sea region (Fig. 11).

Shelf-slope-rise correlations are in general difficult to pursue on most margins because of stacked down-slope transport processes. We selected the highest quality shelf-slope seismic profile nearest to our AS–RS transect whilst being aware of the large uncertainties. It would be desirable, but beyond the scope of this paper, to focus on a more constrained shelf-to-slope stratigraphy correlation of the eastern Ross Sea in a separate study, with more seismic lines and possible future drill sites.

4.2.3. Eastern Amundsen Sea link

Line AWI-20100117 forms the far eastern part of the AS–RS transect and crosses older seismic lines AWI-94054 and AWI-94050 (Table S2; Gohl et al., 1997; Nitsche et al., 1997, 2000; Uenzelmann-Neben and Gohl, 2012) as well as AWI-20060200 (Figs. 2, 9; Table S2; Gohl, 2007; Uenzelmann-Neben and Gohl, 2012; Kalberg and Gohl, 2014). The base of Unit II in Uenzelmann-Neben and Gohl (2012) correlates to the uPG-T/AS-u3 unconformity, whilst the base of Unit III corresponds to the uT-FG/AS-u6 sequence boundary (Figs. 9, 11). All three units occur throughout and the correlation was recognisable without discrepancies or ambiguities (Fig. 11).

4.3. Sediment thicknesses and deposition volumes

AS-1 is the thickest unit in the central part of the basin (~1.3 km; Table S3) at the Endeavour FZ where it in-fills the rugged block faulted basement (Figs. 3, 4; Fig. S1). It is therefore interpreted as a syn- or post rift sequence (line km 1100 in Fig. 4). Little internal faulting is present and AS-1 seems to drape over the basement. However, it thins towards the basin flanks (~133 m thick) and terminates at the Pahemo Fault in

the west, and against the Proto-Antipodes Fault in the east (Fig. 4; Fig. S1). AS-2 follows the trend of AS-1 but is more uniform in thickness in the centre of the basin (~500 m; Table S3; Fig. 4b and Fig. S2) and levels out above the block-faulted basement topography. It terminates against the Kohiku FZ in the east (Fig. 4b and Fig. S2). In contrast, AS-3 is anomalously thick in the east where the levee-drift is located (680 m at point 6, Fig. 4b; Fig. S2) and thins to 108 m thick in the west. But, similarly to AS-2, it terminates at the Kohiku FZ.

AS-4 varies from 155 to 360 m thick (Table S3 and Fig. S2) and thins noticeably upslope (Fig. 4b; Fig. S2). Similar to AS-4, units AS-5, AS-6 and AS-7 thin above the AS-2 PG-drift location to less than 100 m thick (Table S3; Fig. S2) and then propagate eastward to the buried channel–levee system, where they thicken again. All three units have a maximum thickness of 350–400 m (Table S3; Fig. S2) and are parallel to each other, as well as to the units above and below.

AS-8 varies greatly in thickness throughout the basin (45–179 m thickness; Table S3) and is absent between line km 1750 and 2000 (Fig. 4; Figs. S1, S2). Following the trend of units AS-4 to AS-6, it also thins markedly above the AS-2 drift location (Figs. 4b, 5; Figs. S1, S2). AS-9 and AS-10 are similar in thickness (50–200 m thick; Table S3; Fig. S2) but varies in geometry. Both contain drifts, mostly concentrated near where the Pahemo FZ crosses the transect (Fig. 4b; Fig. S1b). Units AS-4 to AS-10 are continuous along the entire transect, parallel and uniform in thickness up to the region above the anomalous basement topography and the AS-2 PG-drift.

The total sediment thickness ranges from 805 to 3909 m (Table S4; Fig. S2) with the thickest part being in the centre of the basin (Fig. 4; Fig. S1). Under the assumption that all units occur throughout the Amundsen Sea basin extent, an area of 1.2 to 1.4×10^6 km² (Fig. 1), we estimate the total sediment volume at 2.8 to 3.3×10^6 km³ (Table S4; Fig. S2). Similarly, by taking the mean thickness of each 1st order sequence (PG = 1281 m, T = 672 m, FG = 631 m) and the min/max of the basin area, we estimate the pre-glacial, transitional and full glacial sediment volumes as: PG = 1.5 to 1.8×10^6 km³, T = 0.8 to 1.0×10^6 km³ and FG = 0.8 to 0.9×10^6 km³ (Table S4; Fig. S2). Our presented volumes and age model are first estimates for this region and have large associated uncertainties due to the limited coverage of seismic data and the absence of deep sea drilling constraints in the Amundsen Sea basin.

4.4. Sedimentation rates

Using the sequence age ranges (Fig. 10) and sediment thicknesses (Table S4; Fig. S2) we determined sedimentation rates for the PG, T and FG sequences (Table S4). The age model contains large uncertainties, because borehole age-control is lacking and we therefore only outline the general trend for the first-order sequences. For the total sediment volume of 2.8 to 3.3×10^6 km³ in the Amundsen Sea basin, a min/max sedimentation rate of 1–3 cm/ky is estimated (Table S4). The PG sequence has the lowest min/max sedimentation rate estimate at 0.6–2.1 cm/ky. The rate progressively increases to 1.0–2.5 cm/ky for the T sequence and is the highest for the FG sequence (1.5–3.6 cm/ky).

5. Discussion

5.1. Oceanic basement off the Amundsen Sea margin

Oceanic basement age is one of the better-constrained parameters for our seismic stratigraphic model of the Amundsen Sea continental rise. Basement age in the Amundsen Sea basin (Wobbe et al., 2012) becomes increasingly younger from 84 Ma (C34y) in the east to 42 Ma (C20n) in the northwest (Fig. 2). In our stratigraphic age model, the selected 12 points along the AS–RS transect range in basement age from 79.5 Ma at point 12 in the east, to 64.6 Ma at point 1 in the west (Figs. 4b, 10; Fig. S1). Therefore, sediments in direct contact with the

basement from transect line km 500 to 2000 (unit AS-1) should be as old as 79.5–64 Ma.

The acoustic basement can generally be divided into four regions based on their distinct structural characteristics. (i) The transect segment from the eastern Ross Sea up to the Kohiku FZ (line km 0–650 in Fig. 4; Fig. S1) shows a rugged and irregular topography, possibly associated with a decrease in spreading rates from 74 to 22 mm/yr, between chrons 27 and 22 (63–50 Ma) (Wobbe et al., 2012; Fig. 2). Such low spreading rates are often described as the mechanism to generate rough basement surfaces (e.g. Malinverno, 1991; Small and Sandwell, 1989). (ii) From the Kohiku FZ to the Endeavour FZ (line km 650–1200 in Fig. 4; Fig. S1), the basement deepens and exhibits major faulting, possibly associated with a number of previous fracture zones in the late Cretaceous oceanic crust. (iii) From the Endeavour FZ to the Proto-Antipodes FZ (line km 1200–1650 in Fig. 4; Fig. S1), the basement topography is relatively smooth and no faults are visible. The top-of-basement has an east–west dip angle of about 1° (Fig. 5). A reason for this part of the basement being smoother than that in the west could be that the spreading rates are greater than 60–70 mm/yr for crust as old as 71 Ma (Wobbe et al., 2012). (iv) The basement east of the Proto-Antipodes FZ (line km 1650–2000 in Fig. 4; Fig. S1) exhibits a very rugged and faulted surface. Here, the transect crosses over to the elevated Marie Byrd Seamount (MBS) province with a greatly structured basement, interleaved with magmatic intrusions (Wobbe et al., 2012). Wobbe et al. (2012) also suggest that continental fragments from the breakup process may be embedded in this province.

5.2. Pre-glacial (PG) sequence

Fig. 12 illustrates a conceptualised model, which is a first attempt to transfer our observations along the AS–RS transect into a process model for the WAIS and bottom current development. In the Cretaceous to Paleocene part of the pre-glacial climate regime (up to 55.8 Ma), the major deposition centre is located in the basin centre near the Endeavour FZ (Fig. 12a). Since sediment deposits are thicker on the eastern flank of the basin (up to 1.3 km for AS-1 and 519 m for AS-2, Table S3) we infer that the pre-glacial depo-centre (marked 'dc' in Fig. 12a) was probably supplied from the southeast, possibly by complex river systems that eroded the elevated inland palaeotopography region in West Antarctica (Wilson et al., 2012). These systems could have transported the largest volume of the total sediments (1.5 to 1.8×10^6 km³; Table S4) into the sea at a deposition rate of 0.6–2.2 cm/ky (Table S4). The routes presumably followed palaeotopographic lows, which later formed the flow stream channels of the subsequent ice sheet.

An approximately 80 km wide mound or drift located to the west of the basin centre near the Pahemo FZ (Fig. 12a), lies directly on the 68–65 Ma basement and is constrained to unit AS-2 (Fig. 6c); hence it cannot be older than 67 Ma (Paleocene age). We speculate that an early regional bottom-current circulation possibly caused it, although the Southern Ocean gateways were still closed at that time (Table S1). Huber et al. (2004) suggested the development of a proto-Ross Sea gyre at 55.8 Ma. It was not possible to deduce any current direction information from the geometry, but considering the likely bathymetry (Fig. 1) and basement high to the west, an eastward flow direction is suggested (Fig. 12a).

Close to the Eocene–Oligocene transition, unit AS-3 was deposited with tentative model ages ranging from 57 to 21 Ma, 30 Ma and 34 Ma along the 12 points (Figs. 10, 11, 12b). AS-3 is the thickest unit in the PG sequence (680 m, Table S3) and contains a large, ~3000 m long, almost 400 m high levee-drift (Figs. 4, 5; Fig. S1). The base of the levee-drift (PG drift) terminates at the top boundary of AS-2, at unconformity AS-u2. If we project the last occurrence of AS-2 onto the timescale (Fig. 10), the base of the drift should be at least younger than 57–40 Ma, thereby placing it in the Eocene (Figs. 10, 11, 12b). The stoss side of the drift trends west (Fig. 5) and this geometry

suggests a bottom-current flow from west to east (Fig. 12b; Stow et al., 2002; Shanmugam, 2006; Shanmugam and Camerlenghi, 2008). The occurrence of a larger and additional PG drift at >55.8 Ma (Figs. 6c, 12a) supports our hypothesis that bottom-current circulation may have already been active in the Eocene and probably earlier, which is consistent with the findings of Uenzelmann-Neben and Gohl (2012). They observe drifts in Unit I (60–21 Ma) near the Marie Byrd Seamounts in the eastern Amundsen Sea, which also implies Paleogene bottom-current activity in this part of the basin. They infer that the likely cause and driving force were related to proto-Antarctic Bottom Water (AABW) deflected against a basement high. The latter is thought to have been caused by thermal uplift related to the emplacement of the Marie Byrd Seamount province. This may explain why it is the only drift in unit AS-3 and at this particular location, which indicates a shift of the PG depo-centre to the east (Fig. 12b).

5.3. Transitional (T) sequence: first WAIS advances to the shelf

The seismic stratigraphy established on the continental rise off Wilkes Land identified the first arrival of the EAIS to the margin at 33.5–30 Ma, marked by the regional unconformity WL-U3 (Fig. 11; Escutia et al., 2011). Comparing the type sections for the Amundsen Sea basin with the seismic line that crosses on IODP Leg 318, Site U1356 (De Santis et al., 1995, 2003; Escutia et al., 2005, 2011), it is visually evident that the lower seismic sequences are similar in amplitude, geometry and seismic character. We thus tentatively correlate our interpreted end of the pre-glacial sequence unconformity AS-u3/uPG-T to unconformity WL-U3 (Fig. 11). The WL-U3 age is in good agreement with our estimated AS-u3/uPG-T model horizon age of 34–28 Ma for the basin flanks (Figs. 10, 11).

From the seismic reflection shelf-slope-rise correlation between the TAN-2006-06 line and drill records of DSDP Leg 28 Sites 270–274, the pre-glacial sequence unconformity AS-u3/uPG-T is tentatively linked to unconformity RSU6 (Figs. 8 and 11). RSU6 has an age range of 34–29 Ma (Brancolini et al., 1995; De Santis et al., 1999; Brancolini and Leitchenkov, 2010; DSDP 270; Fig. 11). Our hypothetical model age of 34–30 Ma for the AS-u3/uPG-T horizon (Figs. 8, 10 and 11), broadly falls within the RSU6 age range given the variation in shelf and slope processes, the large uncertainties in our age model, and the absence of drilling information to constrain the age of AS-u3/uPG-T. We further speculate that the younger trend in the centre (~21 Ma; Fig. 11) may be associated with a delay in the arrival of the ice sheet along this part of the shelf, conceivably due to elevated topography such as a mountain range that it had to overcome before reaching the coast and shelf. The reconstructed 34 Ma maximum palaeotopography model of West Antarctica does suggest an elevated land area opposite the centre of the transect (Wilson et al., 2012), though the possible doming effect of Marie Byrd Land (e.g. LeMasurier, 2008) has not been taken into account. The minimum model however, included an elliptical dome with up to 1000 m of uplift. Alternatively, low-lying palaeo-river drainage systems from the PG climate regime may have redirected the ice streams and drainage towards basin flanks instead.

In the eastern Amundsen Sea, the pre-glacial sequence unconformity AS-u3/uPG-T on line AWI-20100117 of the AS-RS transect, matches the base of Unit II in crossing line AWI-95054 (Figs. 2, 9, 11). The base of Unit II was assigned a hypothetical age of 21 Ma in Uenzelmann-Neben and Gohl (2012) by a jump-correlation to the Ross Sea shelf horizon ages in De Santis et al. (1995). Our age-model however suggests an older age of at least early Oligocene, 30–28 Ma (Figs. 10 and 11). The Eocene–Oligocene transition age of 34 Ma for the uPG-T in our age model and in Leg 318, Site U1356 (Escutia et al., 2005, 2011) is favoured above the younger DSDP ages, because of its similar distal setting and thus assumed similar processes. Based on the seismic horizon mapping, the constructed age model (Figs. 10, 11) and borehole information, we therefore infer an age of about 34 Ma as the suggested timing of the first arrival of glaciers to parts of the coast, which is consistent with

the reconstructed high palaeotopography of West Antarctica (Wilson et al., 2012) and the inferred extent of a modelled ice sheet at that time (Wilson et al., 2013).

By the late Oligocene to mid-Miocene, the deep-water Tasmanian and Drake Passage/Scotia Sea gateways had opened permanently, enabling a constant flow of the ACC (Fig. 12c, Table S1). Seismic records from various Antarctic margins indicate that from the mid-Miocene onward, ice sheets grounded more frequently on the continental shelf and pushed sediments across the slope to form progradational shelf sequences (e.g. De Santis et al., 1999; Brancolini and Leitchenkov, 2010; Gohl et al., 2013). This is in agreement with higher amplitudes and strong reflectivity seen in units AS-4, -5 and -6 above AS-u3/uPG-T (Figs. 4, 6; Fig. S1), which we associate with a larger sediment influx of poorly sorted material such as debris transported onto the rise through downslope processes, and an increase in the sedimentation rate to 1–2.5 cm/ky (Table S4).

In the Ross Sea shelf-slope-rise seismic horizon correlation (Fig. 8), the 26–18 Ma units AS-4 to AS-6 of our transitional regime, match well with units RSS-4a to RSS-3 of the Ross Sea (Brancolini et al., 1995; De Santis et al., 1999), and with WL-S5 at the Wilkes Land margin (Fig. 11; Escutia et al., 2011). In the eastern Amundsen Sea seismic horizon correlation (Fig. 9), AS-4 to AS-6 collectively correlates to Unit II of Uenzelmann-Neben and Gohl (2012) but with a slightly older age range of 30–15 Ma for the eastern Amundsen Sea basin flank (Figs. 10 and 11). However, stratigraphic information from drill holes is absent in the Amundsen Sea and western Bellingshausen Sea and implies large uncertainties in both our and Uenzelmann-Neben and Gohl's (2012) chrono-stratigraphic models.

Sediment drifts occur on the western flank of the basin on a basement high (Figs. 4, 6b; Fig. S1). The amalgamated base of the mounds/drifts lies on AS-u4, in AS-5, as well as on the basement, hence their ages should be at least younger than the youngest age of AS-4, which is 26–24 Ma (Figs. 4b, 6b, 10; Fig. S1). ODP Leg 178 Site 1095 reached sequences of this mid-Miocene age in an ice-distal drift deposit near the Antarctic Peninsula (e.g. Iwai et al., 2002; Uenzelmann-Neben, 2006). Elongate drifts and levee drifts were mapped in Unit II in the eastern Amundsen Sea in Unit and inferred to be 21–15 Myr old (Uenzelmann-Neben and Gohl, 2012; Fig. 11). This age difference of the same distance-correlated sequences could either be explained by large uncertainties in such a long-distance correlation, or by a change in the timing of the same sedimentation processes along the margin. The latter would imply similar WAIS-triggered sediment flux, but arrival on the shelf time-shifted from the Ross Sea to the Amundsen Sea embayment (Fig. 12c).

5.4. Full glacial (FG) sequence: intensified WAIS dynamics

The seismic stratigraphy work on the ice-distal Wilkes Land continental rise identified WL-U5 as the boundary horizon at which the EAIS grounded on the shelf (Escutia et al., 2011). The age of their horizon is consistent with our estimated AS-u6 horizon age of ~15 Ma for the Amundsen Sea basin flanks (Figs. 10, 11).

In the shelf-slope-rise seismic reflection correlation between the TAN-2006-06 line and DSDP Leg 28 Sites 270–272 of the Ross Sea, the transitional sequence unconformity AS-u6/uT-FG links to RSU4 (Figs. 8, 11). RSU4 has an age of 15–17 Ma, constrained by the DSDP Leg 28 boreholes (Brancolini et al., 1995; De Santis et al., 1999; Brancolini and Leitchenkov, 2010). This age range is again, similar to our model age of ~15 Ma on the basin flanks. The upper boundary of the transitional sequence (horizon uT-FG/AS-u6) follows a similar age trend than uPG-T. We infer that uT-FG/AS-u6 probably appears older on the basin flanks (15.3 Ma; Figs. 10, 11) and younger in the middle (9 Ma; Fig. 10) due to later bottom-water circulation and reworking of the Ross Sea gyre and/or AABW generation.

In the eastern Amundsen Sea, the transitional sequence boundary AS-u6/uT-FG in line AWI-20100117, matches the base of Unit III in

crossing line AWI-95054 (Figs. 2, 9, 11). The base of Unit III was assigned a hypothetical age of 14 Ma (Gohl et al., 1997; Nitsche et al., 1997, 2000; Uenzelmann-Neben and Gohl, 2012), which is similar our model age. Though these ages are almost identical, it is a yet unproven hypothesis that needs to be tested by drilling.

From the Miocene to the Pliocene–Pleistocene, the ACC developed fully, bottom water formation and circulation intensified, and the topography of West Antarctica evolved close to the present situation (Fig. 12c,d). After the mid-Miocene, the WAIS advanced across most of the continental shelves in times of glacial maxima (Fig. 12d). This period sees the highest sedimentation rate (1.5–3.6 cm/ky), probably due to the frequent advance/retreat cycles on the shelves. The seismic reflections show complex internal formation geometry, which is an indication for dynamic sediment influx and intensified bottom-current activity (Figs. 4, 6a; Fig. S1).

Our model ages of ~9 to 12 Ma, ~5 Ma and ~1 to 2 Ma for AS-u7, -8 and -9, respectively, are in good agreement with the DSDP Leg 28 drilling data and the seismic chrono-stratigraphy of the Ross Sea shelf (Figs. 8, 10, 11). In the eastern Amundsen Sea, seismic units AS-7 and AS-8 correlate with Unit III, whilst AS-9 and AS-10 correlate with Unit IV (Figs. 9–11), although our age model suggests an older age of 8 Ma as opposed to 4 Ma proposed by Uenzelmann-Neben and Gohl (2012). However, given the large uncertainties in age estimates in long-distance seismic correlation, and the absence of drilling information to support an age model, the differences are within reasonable range. The units are relatively thick along the eastern basin flank (Fig. 4; Figs. S1, S2), which is consistent with depo-centres identified by Uenzelmann-Neben and Gohl (2012). This deposition geometry probably formed due to the close proximity to the glacial outlets of the Amundsen Sea Embayment (red arrows in Fig. 1).

A series of stacked drifts lie on unconformity AS-u9. The stoss side of all the drifts trend west, suggesting an eastward flowing current (Stow et al., 2002; Shanmugam, 2006; Shanmugam and Camerlenghi, 2008), which is in agreement with the post mid-Miocene (<15.5 Ma) bottom-current directions in Uenzelmann-Neben and Gohl (2012). The bases of the FG drifts in unit AS-8 are estimated to be ~9 to 7 Ma, those in AS-9 in the ~8 to 4 Ma age range, and the ones in AS-10, younger than ~4 Ma (Figs. 4b, 10; Fig. S1). The drifts and stacked buried channel–levee systems in all the upper units (Fig. 4; Fig. S1), indicate that sedimentation transport and deposition processes of the Amundsen Sea continental rise occurred in an intense, dynamic and variable manner throughout the late Miocene, Pliocene and Quaternary. Most sediment was likely supplied by the major ice stream outlets of the Amundsen Sea Embayment to the southeast, and the Ross Sea region to the southwest.

5.5. Geodynamic implications for Marie Byrd Land

An interesting observation in the central Amundsen Sea rise is the down-to-west dip of the basement and the lower to middle sedimentary sequences, AS-1 to AS-3, deposited parallel to it (Fig. 5). Above AS-u3, the reflections become increasingly tapered, reaching their largest internal angles up to AS-u6, and then change to progressively more horizontal and parallel above AS-u6 (Fig. 5b). Subtle low-angle onlaps in the internal geometry of the second order sequences (e.g. AS-6 in Fig. 5b) lead us to speculate that this change in horizon angles may be attributed to tectonic uplift. Alternatively, we cannot rule out that subsidence may be one of the possibilities for the implied vertical motion. The negative anomaly in the basement residuals, modelled by Wobbe et al. (2014), and the deep Amundsen Sea basin geometry (Fig. 4; Fig. S1) collectively indicate some degree of local subsidence that may have been controlled by mantle processes. The sequences up to AS-u2 were either present before the uplift, or, the rate of uplift or subsidence was similar to the rate of deposition. The angle changes gradually towards AS-u3, indicating that uplift/subsidence may have initiated and accelerated up to AS-u6. Then, uplift or subsidence may have

stopped and the units above AS-u6 deposited in a horizontal-parallel manner. Imposing our horizon age model on these observations, we imply that the start of vertical movement occurred before or near AS-u3/uPG-T at about 30 Ma and continued until AS-u6/uT-FG at about 13 Ma, when the rate of a tectonic episode slowed down significantly. The down-to-west dip could be related to the elevated Marie Byrd Sea-mount province to the east, which was emplaced by thermally driven magmatic intrusions and underplating of the crust as a product of partial melting (Kalberg and Gohl, 2014; Kipf et al., 2014). Kipf et al. (2014) however, derived an emplacement age of 65–56 Ma for the sea-mounts, which is about 20 myrs before our estimated initiation of the uplift. Instead, we speculate that increasing dynamic topography gradually tilted the area shown in Fig. 5, resulting in the change in horizon dip angles. Such tilting may perhaps be related to the Marie Byrd Land uplift caused by a mantle plume (e.g. LeMasurier, 2008). LeMasurier (2008) estimated the beginning of the MBL uplift to be at about 30–25 Ma, which broadly agrees with our postulated uplift age range. Uplift could have also caused simultaneous subsidence of the adjacent over-deepened western Amundsen Sea basin, in response to lithospheric bulging. However, without mantle-dynamic modelling, the extent and timing of the MBL uplift remain far from being constrained.

6. Conclusions

Our collective interpretation of a continuous Amundsen Sea to Ross Sea seismic transect and supporting seismic lines, enhances the understanding of the Cretaceous to present Amundsen Sea continental rise pre-glacial to full-glacial sedimentation processes. The major seismic units (AS-1 to AS-10) and unconformities (AS-u1 to AS-u9) were grouped into three first order sequences, related to the pre-glacial (PG), transitional (T) and full glacial (FG) climate regimes of Antarctica.

The PG sequence comprises units AS-1 to AS-3, bounded by the basement and unconformity AS-u3/uPG-T, with an age range of ~79 to 34 Ma. AS-3 is thicker than all the other units and contains a large, ~300 km long and up 400 m high, elongated levee drift on the eastern basin flank. It is estimated to be of Eocene age and an eastward flowing Paleocene to Eocene bottom current is inferred from its geometry. The PG sequence is 358–2203 m thick with an estimated sedimentation rate of 0.6–2.1 cm/ky.

The T sequence (units AS-4 to AS-6) has a collective age range of ~34 to 16 Ma and is present throughout the basin, from the Ross Sea to the eastern Amundsen Sea. Sediment drifts, mounds and sediment waves were identified and these are mostly confined to the far western basin flank, perched on a basement high. However, the geometry does not allow for a current direction interpretation on this scale. The T sequence ranges in thickness from 274 to 1070 m, thins from west to east and has an estimated sedimentation rate of 1.0–2.5 cm/ky, which is only slightly higher than that for the PG sequence. This transitional sequence is interpreted to indicate the Late Eocene onset of a glacially dominated environment of West Antarctica.

The FG sequence (units AS-7 to AS-10) ranges in age from ~16 to 0 Ma and is present along the whole transect length, throughout the Ross Sea and Amundsen Sea basins. Sediment drifts are typically 50–100 km wide and 200–300 m high. These are mainly concentrated on the western flank of the basin and are stacked above the Pahemo FZ. The FG drifts' stoss sides pinch out to the west, thus a strong eastward flowing, mid-Miocene to Pliocene bottom-current can be inferred. AS-8 is the only FG unit that has a drift body on the eastern basin flank of the Amundsen Sea basin. The FG sequence sediment thickness ranges from 374 to 889 m and has the highest sedimentation rate (1.5–3.6 cm/ky) compared to the PG and T sequences.

During the pre-glacial to glacial periods, the major deposition centres remained in the basin centre and in front of Ross Sea outlet. No apparent shift in deposition, or change in deep-sea sediment transport processes between the Amundsen Sea and Ross Sea, is obvious.

The seismic sections show continuous sequences with consistent internal geometry and drifts in the centre, and on both basin flanks.

The progressive change in horizon dip in the eastern part of the AS–RS transect, near the Pahemo Fracture Zone, may be attributed to vertical tectonics such as the Marie Byrd Land uplift, or magmatism during the emplacement of the Marie Byrd Seamounts.

The sediment rates and sediment rate changes, temperate versus cold-polar regime, age of onset of glaciation, onset and direction of bottom currents, as well as mapping the spatial distribution of the sequences, volume and depocentre shift extrapolations are currently constrained by good quality data, and the only available in this region. Our continuous seismic sections, the models, ages and rates can thus be viewed as an initial regional framework. Future model improvement can only be obtained by drilling and additional regional seismic data acquisition.

Supplementary data to this article can be found online at <http://dx.doi.org/10.1016/j.palaeo.2015.11.017>.

Acknowledgements

The authors are grateful for the support of the masters and crews of RV *Polarstern* during expedition ANT-XXVI/3 (AWI-2010) and of RV *Tangaroa* during expedition TAN0602 (TAN-2006). We extend our thanks to the seismic teams on board of both vessels for successful data acquisition. The German component of this project was funded by Priority Program 1158, *Antarctic Research*, of the Deutsche Forschungsgemeinschaft (DFG) under project number GO 724/10-1, and by AWI institutional funds from Work Package 3.2 of the AWI Research Programmes PACES and PACES-II. The Government of New Zealand funded the 2006 data acquisition by RV *Tangaroa*. This project contributes to the Research Program *Past Antarctic Ice Sheet Dynamics* (PAIS) of the Scientific Committee on Antarctic Research (SCAR). Seismic data of the Ross Sea shelf were obtained with thanks from the SCAR Antarctic Seismic Data Library System (SDLS). We thank reviewers Laura De Santis and Doug Wilson for their constructive comments and suggestions, which improved the manuscript.

References

- Anderson, J.B., Bartek, L.R., 1992. Cenozoic glacial history of the Ross Sea revealed by intermediate resolution seismic reflection data combined with drill site information. In: Kennett, J.P., Wamke, D.A. (Eds.), *The Antarctic Palaeoenvironment: A Perspective on Global Change, Part One* Antarctic Research Series 56. American Geophysical Union, Washington, DC, pp. 231–263.
- ANTOSTRAT, 1995. Seismic Stratigraphic Atlas of the Ross Sea. In: Cooper, A.K., Barker, P.F., Brancolini, G. (Eds.), *Geology and Seismic Stratigraphy of the Antarctic Margin* 68. American Geophysical Union, Washington, D.C., p. 22 (plates).
- Arndt, J.E., Schenke, H.W., Jakobsson, M., Nitsche, F.-O., Buys, G., Goleby, B., Rebesco, M., Bohoyo, F., Hong, J.K., Black, J., Greku, R.K., Udintsev, G.B., Barrios, F., Reynoso-Peralta, W., Taisei, M., Wigley, R., 2013. The International Bathymetric Chart of the Southern Ocean Version 1.0—a new bathymetric compilation covering circum-Antarctic waters. *Geophys. Res. Lett.* 40 (9), 1–7.
- Bamber, J.L., Riva, R.E.M., Vermeersen, B.L.A., LeBrocq, A.M., 2009. Reassessment of the potential sea-level rise from a collapse of the West Antarctic Ice Sheet. *Science* 324, 901–903. <http://dx.doi.org/10.1126/science.1169335>.
- Barker, P.F., Camerlenghi, A., Acton, G.D., Ramsay, A.T.S., et al., 2002. Proceedings of the ODP. *Sci. Results* 178, 1–40 (www-odp.tamu.edu/publications/178_SRN and www-odp.tamu.edu/publications/178_SR/178OTC.HTM).
- Bart, P.J., 2003. Were West Antarctic Ice Sheet grounding events in the Ross Sea a consequence of East Antarctic Ice Sheet expansion during the middle Miocene? *Earth Planet. Sci. Lett.* 216, 1–2. [http://dx.doi.org/10.1016/S0012-821X\(03\)00509-0](http://dx.doi.org/10.1016/S0012-821X(03)00509-0) (93–107, ISSN 0012-821X).
- Bijl, P.K., Bendle, J.A.P., Bohaty, S.M., Pross, J., Schouten, S., Tauxe, L., Stickle, C.E., McKay, R.M., Röhl, U., Olney, M., Sluijs, A., Escutia, C., Brinkhuis, H., 2013. Eocene cooling linked to early flow across the Tasmanian Gateway. *PNAS* <http://dx.doi.org/10.1073/pnas.1220872110>.
- Brancolini, G. and Leitchenkov, G., 2010. Ross Sea. 118–128. In: Cooper, A.K., Brancolini, G., Escutia, C., Kristoffersen, Y., Larter, R., Leitchenkov, G., O'Brien, P., Jokat, W., 2009. Chapter 5 - Cenozoic Climate History from Seismic Reflection and Drilling Studies on the Antarctic Continental Margin. In: Florindo, F., Siegert, M. (Eds.), *Developments in Earth and Environmental Sciences 8, Antarctic Climate Evolution*. Elsevier, 115–228.
- Brancolini, G., Cooper, A.K., Coren, F., 1995. *Seismic Facies and Glacial History in the Western Ross Sea (Antarctica)*. Antarctic Research Series 68. American Geophysical Union, pp. 209–234 (Washington, DC).
- Cande, S.C., Stock, J.M., Müller, R.D., Ishihara, T., 2000. Cenozoic motion between East and West Antarctica. *Nature* 404, 145–150. <http://dx.doi.org/10.1038/35004501>.
- Davey, F.J., De Santis, L., 2006. A multi-phase rifting model for the Victoria Land Basin, western Ross Sea. In: Fütterer, D.K., Damaske, D., Kleinschmidt, G., Miller, H., Tessensohn, F. (Eds.), *Antarctica: Contributions to Global Earth Sciences*. Springer-Verlag, pp. 303–308 http://dx.doi.org/10.1007/3-540-32934-X_38.
- De Santis, L., Anderson, J.B., Brancolini, G., Zayatz, I., 1995. Seismic record of late Oligocene through Miocene glaciation on the Central Eastern continental shelf of Ross Sea. In: Cooper, A.K., Barker, P.F., Brancolini, G. (Eds.), *Geology and Seismic Stratigraphy of the Antarctic Margin* Antarctic Research Series 68. American Geophysical Union, Washington, D.C., pp. 235–260.
- De Santis, L., Prato, S., Brancolini, G., Lovo, M., Torelli, L., 1999. The Eastern Ross Sea continental shelf during the Cenozoic: implications for the West Antarctic ice sheet development. *Glob. Planet. Chang.* 23, 173–196. [http://dx.doi.org/10.1016/S0921-8181\(99\)00056-9](http://dx.doi.org/10.1016/S0921-8181(99)00056-9).
- De Santis, L., Brancolini, G., Donda, F., 2003. Seismo-stratigraphic analysis of the Wilkes Land continental margin (East Antarctica): influence of glacially driven processes on the Cenozoic deposition. *Deep-Sea Res. II Top. Stud. Oceanogr.* 50 (8–9), 1563–1594. [http://dx.doi.org/10.1016/S0967-0645\(03\)00079-1](http://dx.doi.org/10.1016/S0967-0645(03)00079-1).
- Eagles, G., Jokat, W., 2014. Tectonic reconstructions for paleobathymetry in Drake Passage. *Tectonophysics* 611, 28–50. <http://dx.doi.org/10.1016/j.tecto.2013.11.021>.
- Eagles, G., Gohl, K., Larter, R.D., 2004a. Life of the Bellingshausen plate. *Geophys. Res. Lett.* 31, L07603. <http://dx.doi.org/10.1029/2003GL019127>.
- Eagles, G., Gohl, K., Larter, R.D., 2004b. High-resolution animated tectonic reconstruction of the South Pacific and West Antarctic margin. *Geochem. Geophys. Geosyst.* 5, Q07002. <http://dx.doi.org/10.1029/2003GC000657>.
- Escutia, C., Eittrheim, S.L., Cooper, A.K., Nelson, C.H., 2000. Morphology and acoustic character of the Antarctic Wilkes Land turbidite system: icesheet-sourced versus river-sourced fans. *J. Sediment. Res.* 70 (1), 84–93. <http://dx.doi.org/10.1306/2DC40900-0E47-11D7-8643000102C1865D>.
- Escutia, C., De Santis, L., Donda, F., Dunbar, R.B., Cooper, A.K., Brancolini, G., Eittrheim, S.L., 2005. Cenozoic ice sheet history from East Antarctic Wilkes Land continental margin sediments. *Glob. Planet. Chang.* 45, 51–81. <http://dx.doi.org/10.1016/j.gloplacha.2004.09.010>.
- Escutia, C., Brinkhuis, H., Klaus, A., Expedition 318 Scientists, 2011. Proceedings IODP, 318. Integrated Ocean Drilling Program Management International, Inc., Tokyo <http://dx.doi.org/10.2204/iodp.proc.318.2011> (101 pp.).
- Fretwell, P., et al., 2013. *Bedmap2: improved ice bed, surface and thickness datasets for Antarctica*. *Cryosphere* 7, 375–393.
- Gohl, K., 2007. The Expedition ANTARKTIS-XXIII/4 of the Research Vessel “Polarstern” in 2006. *Berichte zur Polar- und Meeresforschung (Reports on Polar and Marine Research)* 557 (166 pp., <http://epic.awi.de/26756/>).
- Gohl, K., 2010. The expedition of the research vessel “Polarstern” to the Amundsen Sea, Antarctica, in 2010 (ANT-XXVI/3). *Rep. Polar Mar. Res.* 617 (<http://epic.awi.de/29635/>).
- Gohl, K., Nitsche, F., Vanneste, K., Miller, H., Fechner, N., Oszko, L., Hübscher, C., Weigelt, E., Lambrecht, A., 1997. Tectonic and sedimentary architecture of the Bellingshausen and Amundsen Sea Basins, SE Pacific, by seismic profiling. In: Ricci, C.A. (Ed.), *The Antarctic Region: Geological Evolution and Processes*. Terra Antarctica Publication, Siena, pp. 719–723.
- Gohl, K., Uenzelmann-Neben, G., Larter, R.D., Hillenbrand, C.-D., Hochmuth, K., Kalberg, T., Weigelt, E., Davy, B., Kuhn, G., Nitsche, F.O., 2013. Seismic stratigraphic record of the Amundsen Sea Embayment shelf from pre-glacial to recent times: evidence for a dynamic West Antarctic Ice Sheet. *Mar. Geol.* 344, 115–131. <http://dx.doi.org/10.1016/j.margeo.2013.06.011>.
- Gradstein, F.M., Ogg, J.G., Smith, A.G. (Eds.), 2004. *A Geologic Time Scale 2004*. 610 pp, Cambridge University Press, Cambridge.
- Granot, R., Cande, S.C., Stock, J.M., Davey, F.J., Clayton, R.W., 2010. Postspreading rifting in the Adare Basin, Antarctica: regional tectonic consequences. *Geochem. Geophys. Geosyst.* 11, Q08005. <http://dx.doi.org/10.1029/2010GC003105>.
- Hayes, D.E., Frakes, L.A., Shipboard_Scientific_Party, 1975. A geophysical study of the Ross Sea, Antarctica Sites 270, 271, 272. In: Hayes, D.E., Frakes, L.A. (Eds.), *Initial Reports of the Deep Sea Drilling Project, Leg 28*. U.S. Government Printing Office, Washington, D.C., pp. 211–334 (887–907).
- Haywood, A.M., Smellie, J.L., Ashworth, A.C., Cantrill, D.J., Florindo, F., Hambrey, M.J., Hill, D., Hillenbrand, C.-D., Hunter, S.J., Larter, R.D., Lear, C.H., Passchier, S., van de Wal, R., 2009. Chapter 10—Middle Miocene to Pliocene History of Antarctica and the Southern Ocean. In: Florindo, F., Siegert, M. (Eds.), *Developments in Earth and Environmental Sciences 8, Antarctic Climate Evolution*. Elsevier, The Netherlands, pp. 401–463.
- Hinz, K., Block, M., 1985. Results of geophysical investigations in the Weddell Sea and in the Ross Sea. *Proceedings of the 11th World Petrologic Congress, London 1983*. *Geology Exploration Reserves 2*. John Wiley and Sons, New York.
- Huber, M., Brinkhuis, H., Stickle, C.E., Döös, K., Sluijs, A., Warnaar, J., Schellenberg, S.A., Williams, G.L., 2004. Eocene circulation of the Southern Ocean: was Antarctica kept warm by subtropical waters? *Paleoceanography* 19, PA4026. <http://dx.doi.org/10.1029/2004PA001014>.
- Iwai, M., Acton, G., Lazarus, D., Osterman, L.E., Williams, T., 2002. Magnetobiochronological Synthesis of ODP Leg 178 Rise Sediments from the Pacific Sector of the Southern Ocean: Sites 1095, 1096, and 1101. In: Barker, P.F., Camerlenghi, A., Acton, G.D., Ramsay, A.T.S. (Eds.), *Proceedings of the Ocean Drilling Program Scientific Results 178, Ocean Drilling Program, College Station*.
- Jordan, T.A., Ferraccioli, F., Vaughan, D.G., Holt, J.W., Corr, H., Blankenship, D.D., Diehl, T.M., 2010. Aerogravity evidence for major crustal thinning under the Pine Island Glacier

- region (West Antarctica). *GSA Bull.* 122 (5–6), 714–726. <http://dx.doi.org/10.1130/B26417.1>.
- Kalberg, T., Gohl, K., 2014. The crustal structure and tectonic development of the continental margin of the Amundsen Sea Embayment, West Antarctica: implications from geophysical data. *Geophys. J. Int.* 198, 327–341. <http://dx.doi.org/10.1093/gji/ggu118>.
- Kipf, A., Hauff, F., Werner, R., Gohl, K., van den Bogaard, P., Hoernle, K., Maicher, D., Klügel, A., 2014. Seamounts off the West Antarctic margin: a case for non-hotspot driven intraplate volcanism. *Gondwana Res.* 25, 1660–1679. <http://dx.doi.org/10.1016/j.gr.2013.06.013>.
- Larter, R.D., Cunningham, A.P., Barker, P.F., Gohl, K., Nitsche, F.O., 2002. Tectonic evolution of the Pacific margin of Antarctica 1. Late Cretaceous tectonic reconstructions. *J. Geophys. Res.* 107 (B12), 2345. <http://dx.doi.org/10.1029/2000JB000052>.
- Leitchenkov, G.L., Guseva, Y.B., Gandyukhin, V.V., 2007a. Cenozoic environmental changes along the East Antarctic continental margin inferred from regional seismic stratigraphy. In: Cooper, A.K., Raymond, C.R. (Eds.), *Antarctica: A Keystone in a Changing World—Online Proceedings of the 10th ISAES: USGS Open-File Report 2007–1047*. Short Research Paper 005 <http://dx.doi.org/10.3133/of2007-1047.srp005>.
- Leitchenkov, G.L., Gandyukhin, V.V., Guseva, Y.B., 2007b. Crustal structure and evolution of the Mawson Sea, western Wilkes Land margin, East Antarctica. In: Cooper, A.K., Raymond, C.R., et al. (Eds.), *Antarctica: A Keystone in a Changing World—Online Proceedings of the 10th ISAES. USGS Open-File Report 2007–1047*, Short Research Paper 028 <http://dx.doi.org/10.3133/of2007-1047.srp028>.
- Leitchenkov, G., Guseva, J., Gandyukhin, V., Griukurov, G., Kristoffersen, Y., Sand, M., Golynsky, A., Aleshkova, N., 2008. Crustal structure and tectonic provinces of the Riiser Larsen Sea area (East Antarctica): results of geophysical studies. *Mar. Geophys. Res.* 29, 135–158. <http://dx.doi.org/10.1007/s11011-008-9051-z>.
- LeMasurier, W.E., 2008. Neogene extension and basin deepening in the West Antarctic rift inferred from comparisons with the East African rift and other analogs. *Geology* 36, 247–250. <http://dx.doi.org/10.1130/G24363A>.
- Lindeque, A., Martin, Y.M., Gohl, K., Maldonado, M., 2013. Deep-sea pre-glacial to glacial sedimentation in the Weddell Sea and southern Scotia Sea from a cross-basin seismic transect. *Mar. Geol.* 336, 61–83. <http://dx.doi.org/10.1016/j.margeo.2012.11.004>.
- Luyendyk, B., Wilson, D.S., Siddoway, C.S., 2003. Eastern margin of the Ross Sea Rift in western Marie Byrd Land, Antarctica: crustal structure and tectonic development. *Geochem. Geophys. Geosyst.* 3, 4. <http://dx.doi.org/10.1029/2002GC000462>.
- Maldonado, A., Bohoyo, F., Galindo-Zaldívar, J., Hernández-Molina, F.J., Jabaloy, A., Lobo, F.J., Rodríguez-Fernández, J., Suriñach, E., Vázquez, J.T., 2006. Ocean basins near the Scotia–Antarctic plate boundary: influence of tectonics and paleoceanography on the Cenozoic deposits. *Mar. Geophys. Res.* 27, 83–107. <http://dx.doi.org/10.1007/s11001-006-9003-4>.
- Malinverno, A., 1991. Inverse square-root dependence of mid-ocean-ridge flank roughness on spreading rate. *Nature* 352 (6330), 58–60. <http://dx.doi.org/10.1038/352058a0>.
- Miller, K.G., Wright, J.D., Katz, M.E., Browning, J.V., Cramer, B.S., Wade, B.S., Mizintseva, S.F., 2008. A view of Antarctic ice-sheet evolution from sea-level and deep-sea isotope changes during the Late Cretaceous–Cenozoic. In: Cooper, A.K., Barrett, P.J., Stagg, H., Storey, B., Stump, E., Wise, W., 10th ISAES editorial team (Eds.), *Proceedings of the 10th International Symposium on Antarctic Earth Sciences. Antarctica: A Keystone in a Changing World*. The National Academies Press, Washington, DC <http://dx.doi.org/10.3133/of2007-1047.kp06>.
- Nitsche, F.O., Gohl, K., Vanneste, K., Miller, H., 1997. Seismic expression of glacially deposited sequences in the Bellingshausen and Amundsen Seas, West Antarctica. In: Barker, P.F., Cooper, A.K. (Eds.), *Geology and Seismic Stratigraphy of the Antarctic Margin 2 Antarctic Research Series 71*. American Geophysical Union, Washington, D.C., pp. 95–108.
- Nitsche, F.O., Cunningham, A.P., Larter, R.D., Gohl, K., 2000. Geometry and development of glacial continental margin depositional systems in the Bellingshausen Sea. *Mar. Geol.* 162 (2–4), 277–302.
- Olivetti, V., Balestrieri, M.L., Rossetti, F., Thomson, S.N., Talarico, F.M., Zattin, M., 2015. Evidence of a full West Antarctic Ice Sheet back to the early Oligocene: insight from double dating of detrital apatites in Ross Sea sediments. *Terra Nova* 27 (3), 238–246. <http://dx.doi.org/10.1111/ter.12153>.
- Pritchard, H.D., Ligtenberg, S.R.M., Fricker, H.A., Vaughan, D.G., van der Broeke, M.R., Padman, L., 2012. Antarctic ice-sheet loss driven by basal melting of ice shelves. *Nature* 484, 502–505. <http://dx.doi.org/10.1038/nature10968>.
- Rebesco, M., Hernández-Molina, F.H., Van Rooij, D., Wählin, A., 2014. Contourites and associated sediments controlled by deep-water circulation processes: state-of-the-art and future considerations. *Mar. Geol.* <http://dx.doi.org/10.1016/j.margeo.2014.03.011>.
- Rogenhagen, J., Jokat, W., Hinz, K., Kristoffersen, Y., 2004. Improved seismic stratigraphy of the Mesozoic Weddell Sea. *Mar. Geophys. Res.* 25, 265–282. <http://dx.doi.org/10.1007/s11001-005-1335-y>.
- Scheuer, C., Gohl, K., Eagles, G., 2006. Gridded isopach maps from the South Pacific and their use in interpreting the sedimentation history of the West Antarctic continental margin. *Geochem. Geophys. Geosyst.* 7, Q11015. <http://dx.doi.org/10.1029/2006GC001315>.
- Shanmugam, G., 2006. *Deep-water processes and facies models. Handbook of Petroleum Exploration and Production 5*. Elsevier, Amsterdam (476 pp.).
- Shanmugam, G., Camerlenghi, M.R.A., 2008. Chapter 5 Deep-water bottom currents and their deposits. In: Rebesco, M., Camerlenghi, A. (Eds.), *Contourites, Developments in Sedimentology 60*. Elsevier, Oxford, Great Britain, pp. 59–81. [http://dx.doi.org/10.1016/S0070-4571\(08\)00205-7](http://dx.doi.org/10.1016/S0070-4571(08)00205-7).
- Small, C., Sandwell, D.T., 1989. An abrupt change in ridge axis gravity with spreading rate. *J. Geophys. Res. Solid Earth* 94 (B12), 17383–17392. <http://dx.doi.org/10.1029/JB094iB12p17383>.
- Stow, D.A.V., Faugères, J.-C., Howe, J.A., Pudsey, C.J., Viana, A.R., 2002. *Bottom currents, contourites and deep-sea sediment drifts: current state-of-the-art*. In: Stow, D.A.V., Pudsey, C.J., Howe, J.A., Faugères, J.-C., Viana, A.R. (Eds.), *Deep-water Contourite Systems: Modern Drifts and Ancient Series. Memoir. Geological Society of London*, pp. 7–20 (London).
- Tucholke, B.E., Edgar, N.T., Boyce, R.E., 1976. Physical properties of sediments and correlations with acoustic stratigraphy: Leg 35, Deep Sea Drilling Project. In: Hollister, C.D., Craddock, C. (Eds.), *Initial Reports. Deep Sea Drilling Project*, Washington, D.C., pp. 229–249.
- Uenzelmann-Neben, G., 2006. Depositional patterns at Drift 7, Antarctic Peninsula: along-slope versus down-slope sediment transport as indicators for oceanic currents and climatic conditions. *Mar. Geol.* 233, 49–62. <http://dx.doi.org/10.1016/j.margeo.2006.08.008>.
- Uenzelmann-Neben, G., Gohl, K., 2012. Amundsen Sea sediment drifts: archives of modifications in oceanographic and climatic conditions. *Mar. Geol.* 299–302, 51–62. <http://dx.doi.org/10.1016/j.margeo.2011.12.007>.
- Uenzelmann-Neben, G., Gohl, K., 2014. Early glaciation already during the Early Miocene in the Amundsen Sea, Southern Pacific: indications from the distribution of sedimentary sequences. *Glob. Planet. Chang.* 120, 92–104. <http://dx.doi.org/10.1016/j.gloplacha.2014.06.004>.
- Wannesson, J., Perlas, M., Pettiperrin, B., Perret, M., Segoufin, J., 1985. A geophysical transect of the Adelie margin, East Antarctica. *Mar. Pet. Geol.* 2, 192–201. [http://dx.doi.org/10.1016/0264-8172\(85\)90009-1](http://dx.doi.org/10.1016/0264-8172(85)90009-1).
- Wilson, D.S., Jamieson, S.S.R., Barrett, P.J., Leitchenkov, G., Gohl, K., Larter, R.D., 2012. Antarctic topography at the Eocene–Oligocene boundary. *Palaeogeogr. Palaeoclimatol. Palaeoecol.* 335–336, 24–34. <http://dx.doi.org/10.1016/j.palaeo.2011.05.028>.
- Wilson, D.S., Pollard, D., DeConto, R.M., Jamieson, S.S.R., Luyendyk, B.P., 2013. Initiation of the West Antarctic Ice Sheet and estimates of total Antarctic ice volume in the earliest Oligocene. *Geophys. Res. Lett.* 40, 4305–4309. <http://dx.doi.org/10.1002/grl.50797>.
- Wobbe, F., Gohl, K., Chambord, A., Sutherland, R., 2012. Structure and breakup history of the rifted margin of West Antarctica in relation to Cretaceous separation from Zealandia and Bellingshausen plate motion. *Geochem. Geophys. Geosyst.* 13, Q04W12. <http://dx.doi.org/10.1029/2011GC003742>.
- Wobbe, F., Lindeque, A., Gohl, K., 2014. Anomalous South Pacific lithosphere dynamics derived from new total sediment thickness estimates off the West Antarctic margin. *Glob. Planet. Chang.* 123, 139–149. <http://dx.doi.org/10.1016/j.gloplacha.2014.09.006> (Part A).